DNA Damage Response in Live yeast using Single Molecule Microscopy

Shubhika Ranjan

Supervisor: Dr. Rodrigo Reyes Lamothe

Department of Biology
Faculty of Science
McGill University, Montreal

June 2021

A thesis submitted to McGill University in partial fulfillment of the requirements of the degree of Master of Science

I dedicate this thesis to my mother and my brother – Thank you for your love and support

मैं यह अपनी माँ और अपने भाई को समर्पित करती हूं - आपके प्यार और समर्थन के लिए धन्यवाद

Acknowledgements

First, I would like to thank my supervisor, Dr. Rodrigo Reyes-Lamothe, for making my graduate experience truly exceptional. He has always been my mentor and kept me motivated even when my experiments were not working. He gave me the confidence and freedom to explore ideas that I could potentially use for my experiments. Working with him has strengthened my hope to pursue a life of critical thinking, learning and humility. I am grateful for the trust, kindness and patience at the core of this learning experience.

Second, I would like to thank former and current members of the Reyes Lab. I will always cherish their help and support during my time in the lab. They have an amazing friend and support in the time of the pandemic. I would like to give special thanks to Ziad El-Hajj and Huan Zheng for helping me learn the techniques used in the lab that I have used in my experiments for the thesis. I don't think completing my Masters would have been possible without their constant encouragement.

Next, I would like to thank my committee members, Dr. Maria Vera Ugalde and Dr. Nam-Sung Moon. Their feedback on the project has been instrumental in improving the quality of work and direction. I would also like to thank Dr. Stephanie Weber, whose enthusiasm and insight during lab meetings have been incredibly helpful. I offer my sincere gratitude to the Canadian Institutes of Health Research (CIHR) and the Department of Biology at McGill for granting generous financial support for my research.

I would like to thank my family, especially my mother and my brother, who has always supported me. I want to share my success with them for being my confidant. My brother has always mentored me to reach where I am today. I have endless gratitude for my grandparents and inspired me to work harder towards my passion and always encouraging me. My Aunts and Uncle are always there for me emotionally when I was living miles away from my family. Talking to my Cousins in this time of lockdown is like therapy to me. I want to extend my gratitude to my boyfriend for always believing in me

and helping me work towards achieving my goal. His constant word of motivation means a lot to me.

Lastly, I would like to thank my other family, my friends. They have sustained me, offering space for learning, growth and meaningful support that I did not anticipate. In times of doubt, I never hesitate to talk to them about it, and they never failed in supporting me when I needed them.

Many people both within and beyond the lab have helped me reach where I am today, and I am thankful for this experience.

Contributions of Authors

I performed all data collection and processing for this research project. All work presented in this thesis is my own unless otherwise stated, with feedback from my supervisor, Dr. Rodrigo Reyes-Lamothe.

Dr. Ziad El Hajj and Huan Zheng helped me learn the techniques required for collecting the data for Chapter 4 and Chapter 5. Pim van den Bersselaar, a visiting intern, worked on data collection for Chapter 6. Dr. Nitin Kapadia and Dr. Stephan Uphoff wrote the MATLAB scripts used for single-molecule tracking analysis. I completed the dissection of the strain mentioned in Chapter 4 with the help of Gwenole Paquet, an undergraduate student.

Abstract

The genetic information stored in DNA must be faithfully copied and transmitted to the next generation of cells at every cell cycle. The replication of this genetic information is performed by special multiprotein replication machinery, referred to as “replisome,” which synthesizes both daughter duplexes simultaneously. At times, the accurate replication of the genome can go awry, causing mutations that can lead to a collection of diseases. In eukaryotic cells, detection and response to DNA damage during DNA replication is performed by the DNA damage response (DDR) pathway. DDR uses exposed single-stranded DNA as a signal for DNA damage and proceeds by activation of kinases that transmit the signal and change the cell program to respond to the damage. The overall purpose of this work is to understand how cells do this initial detection and how they make the decision to activate the signalling pathway.

I used budding yeast (*Saccharomyces cerevisiae)*, a unicellular model organism, to understand the eukaryotic genetic architecture because it provides a framework to develop and optimize methods to standardize the analysis. I focus on the study of dynamics of DNA replication and DDR proteins of cells experiencing DNA damage or replication fork stalling using single-molecule microscopy. Although this technique provides a high signal-to-noise ratio for visualization while still retaining the integral features in the physiological context of biological systems, various factors play a major role in attaining such high-quality data for further analysis. In the first part of this work, I provide an overview for optimizing the single-molecule techniques while considering various factors involved. In the second section, I describe the initial work towards visualizing the proteins involved in DNA damage response in HaloTag labelled *S. cerevisiae.*

Résumé

L’information génétique enregistrée dans l'ADN doit être fidèlement copiée et transmise à la prochaine génération de cellules à chaque cycle cellulaire. La réplication de cette information génétique est effectuée par un complexe multiprotéique spécial, nommé «réplisome», qui synthétise les deux brins filles simultanément. Parfois, la réplication précise du génome peut mal tourner, provoquant des mutations qui peuvent conduire à un ensemble de maladies. Dans les cellules eucaryotes, la détection et la réaction aux dommages à l'ADN pendant la réplication de l'ADN sont effectuées par la voie de réponse aux dommages à l'ADN (DDR, DNA Damage Response). DDR utilise un bri simple d’ADN exposé comme un signe de dommage à l'ADN et procède à l'activation de kinases qui transmettent le signal et modifient le programme cellulaire pour répondre aux dommages. L'objectif général de ce travail est de comprendre comment les cellules effectuent cette détection initiale et comment elles prennent la décision d'activer la voie de signalisation.

J'ai utilisé la levure bourgeonnante (*Saccharomyces cerevisiae*), un organisme modèle unicellulaire, pour comprendre l'architecture génétique eucaryote, car cet organisme fournit un cadre pour développer et optimiser des méthodes pour standardiser l'analyse. Je me concentre sur l'étude de la dynamique de la réplication de l'ADN et des protéines DDR de cellules présentant des dommages à l'ADN ou un blocage de la fourche de réplication en utilisant la microscopie à molécule unique. Bien que cette technique offre un rapport signal/bruit élevé pour la visualisation tout en conservant les caractéristiques intégrales dans le contexte physiologique des systèmes biologiques, divers facteurs jouent un rôle majeur dans l'obtention de données de haute qualité pour une analyse ultérieure. Dans la première partie de ce travail, j’offre un aperçu de l'optimisation des techniques à molécule unique tout en considérant les différents facteurs impliqués. Dans la deuxième section, je décris le travail initial visant à visualiser les protéines impliquées dans la réponse aux dommages à l'ADN chez *S. cerevisiae* marqué par HaloTag.

Abbreviations

µl: micro litre

µm: micro meter (microns)

2D: 2 dimension

5-FOA: 5-Fluoroorotic Acid

ATP: Adenosine Tri Phosphate

AU: Arbitrary Unit

BP: Base Pair

CDC45: Cell Division Control protein 45

CDK: Cyclin-Dependent Kinases

CHK1: Checkpoint Kinase 1

CMG: Cdc45-MCM-GINS complex

CoM: Center of Mass

ConA: Concanavalin A

Ctf4: Chromosome Transmission Fidelity 4

DAM: DNA Adenine Methyltransferase enzyme

DDK: Dbf4-dependent Cdc7 kinase

DDR: DNA Damage Response

DMSO: Dimethyl Sulfoxide

DNA: Deoxyribose Nucleic Acid

dNTP: deoxyribonucleotide triphosphate

dsDNA: Double-Stranded DNA

DUN1: DNA-damage UNinducible protein 1

eGFP: enhanced Green Fluorescent Protein

EMCCD: Electron Multiplying CCD(Charged Couple Device)

ER: Endoplasmic Reticulum

FATC: FRAP, ATM, TRRAP C-terminal domain

FCS: Fluorescence Correlation Spectroscopy

FRAP: Fluorescence Recovery After Photobleaching method

G1 phase: Gap1 or Growth1 Phase

GATC: Guanine Adenine Thymine Cytosine

GINS: 5-1-2-3 (Go-Ichi-Ni-San) for Sld5, Psf1, Psf2 and Psf3

gRNA: Guide RNA

H2B-GFP: H2B histone - Green Fluorescent Protein

HILO: Highly Inclined and Laminated Optical Sheet

HU: Hydroxy Urea

hygB: hygromycin B

ICGC: International Cancer Genome Consortium

ILE: Integrated Laser Engine

JF549: Janelia Farms 549

JF552: Janelia Farms 552

JF646: Janelia Farms 646

KAc: Potassium acetate

kan: Kanamycin

KB: Kilo Base

KOD: Potassium deuteroxide solution

LAP: Linear Assignment Problem

latA: LatrunculinA

LB: Luria-Bertani medium

Leu: Leucine

LoG: Laplacian of Gaussian

MCM: Minichromosome maintenance protein complex

min: minute

ml: Milli Litre

mM: Milli Molar

mNG: mNeonGreen

mRNA: Messenger RNA

ms: milli second

MSD: Mean Squared Displacement

MSE: Mean Squared Error

MT: Microtubule

NAG: N-acetylglucosamine

ng: nano gram

nm: nano meter

NT: Nucleotide

OD: Optical Density

ORC: Origin Recognition Complex

PA-JF549: Photo Activable-Janelia Farms

PA-JF646: Photo Activable-Janelia Farms

PAM: Protospacer Adjacent Motif

PCNA: Proliferating cell nuclear antigen

PCR: Polymerase Chain Reaction

PEG: Polyethylene Glycol

pH: Potential of Hydrogen

PI3 kinase: Phosphoinositide 3-kinases

PIKK: Phosphatidylinositol 3-kinase related kinases

Pol α: DNA Polymerase Alpha

Pol δ: DNA Polymerase Delta

Pol ε: DNA Polymerase Epsilon

RFC: Replication Factor C

RNA: Ribo Nucleic Acid

RNase A: Ribonuclease A

RPA: Replication Protein A

RPM: Rotation Per Minute

S. cerevisiae: Saccharomyces cerevisiae

S. pombe: Saccharomyces pombe

S/G2: Synthesis Phase and Gap or growth phase 2

SC: Synthetic complete

sec: seconds

sgRNA: single guide RNA

SIFT: Sorting Intolerant From Tolerant

SMM: Single-Molecule Microscopy

SPC42: Spindle Pole body Component 42

SPT: Single Particle Tracking

sptPALM: Single-particle tracking photoactivated localization microscopy

SSB: Single-Stranded Binding Protein

ssDNA: Single-Stranded DNA

TIRF: Total Internal Reflection Fluorescence Microscopy

Ura- : Uracil

URA3: URAcil requiring genetic region 3

UV: Ultra Violet Rays

WT: Wild Type

YPD: Yeast extract peptone dextrose

Table of Contents

Acknowledgements	IV
Contribution of Authors	VI
Abstract	VII
Résumé	VIII
Abbreviations	IX
Table of Contents	XIV
Chapter 1: Introduction	1
Chapter 2: Literature Review	7-21
• Yeast Biology and DNA Replication	7
• DNA stress and DNA Damage Response	8
• Importance of the study of DDR	10
• How to study DDR in live yeast?	10
• Factors affecting Single-Molecule Microscopy in live yeast	13
• Bioinformatics Analysis of protein involved in DDR	14
• CRISPR-Cas9 for N-terminal fusion of HaloTag	15
• Nuclear movement in yeast	17

- Mathematics Models for analysis 18

Chapter 3: Materials and Methods 22-30

- Plasmid Construction 22
- Primer Designing 22
    - C terminal primers 22
    - N terminal primers 23
- Strain Construction: C terminal yeast transformation 23
- Strain Construction: CRISPR-Cas9 24
- Sample Preparation for Single-Molecule Microscopy 25
- Cleaning Cover Slips 27
- Single-Molecule Microscopy 27
- Analysis of Data 28

Chapter 4: Characterizations and study of DDR dynamics 31-38

- Experimental Approach and Results 31
- Discussion 37

Chapter 5: Factors affecting SMM in yeast 39-48

- Experimental Approach and Results 39
    - Choice of Fluorophores 39
    - Autofluorescence, Cell Wall and Choice of Growth Conditions 44
- Discussion 47

Chapter 6: Effects of Nuclear Movement in yeast and other biological factors affecting the movement 49-55

- Experimental Approach and Results 49
- Discussion 54

Chapter 7: Conclusion 56

References 58

Appendices 66-87

- Appendix I: Yeast Strains 66
- Appendix II: Plasmids 67
- Appendix III: Oligonucleotide Sequences 68
  - For Plasmid Cloning 68
  - For strain construction 69
- Appendix IV: HaloTag Fluorescent dye 71
- Appendix V: Nuclear Movement of yeast Data Analysis 72
- Appendix VI: Factor affecting SMM data analysis 77
- Appendix VII: DDR Data Analysis 85

Chapter 1: INTRODUCTION

Deoxyribonucleic acid, or DNA, is the double-helical hereditary material that stores the genetic information within the cells of our body. The amount of DNA duplicated in an organism directly relates to the transfer of genetic information. Inevitably the process of accurate copying of this genome can go awry, yielding mutations that can affect our lives and lead to a collection of diseases.

The DNA wraps itself around the histone proteins for compaction within the cell's nucleus. The copying process needs to deal with the fact that DNA is folded around these protein complexes and cramped into a volume that creates spatial organization problems of higher order. The DNA-binding proteins also need to be duplicated along with the copying of DNA and the chemical modification concerning DNA and histones.

Several sub-processes combine to provide efficient genome replication. Central to this process is machinery that copies the DNA with high fidelity, including the protein complex that initiates the entire process and the protein complex that replicates one helix to two. Superimposed to this fundamental process is the mechanism that detects and repairs errors and damages to the DNA. In addition, specific specialized proteins in the replication apparatus venture the efficient duplication of histone proteins and their chromatin modification. Finally, another machinery cooperates with the replication apparatus to ensure that the tethering of two sister chromatids together until the replication completes. Only by combining these processes can genetic inheritance ensure that each cell has a faithful copy of its parents' genome.

Initiation of the DNA replication requires the opening of the double-stranded DNA for loading of the replisome. In eukaryotes, this would require an origin of replication on DNA, the protein complex ORC, and other initiation factors, ultimately loading the MCM. Then, after unwinding the helix, the DNA polymerases responsible for DNA synthesis come into the picture. Since DNA polymerase cannot initiate copying of the nucleic acid chain, DNA-dependent RNA polymerase synthesizes primers. Following this, the DNA- dependent

DNA polymerase attaches to the 3’ end of this RNA primer and begins DNA replication. Thus, the replisome, special multiprotein replication machinery, simultaneously synthesizes both daughter duplexes. Replication machines have the same core components in all cells: *DNA polymerase, circular sliding clamps, a pentameric clamp loader, helicase, primase and SSB (Single-stranded binding proteins)* [1].

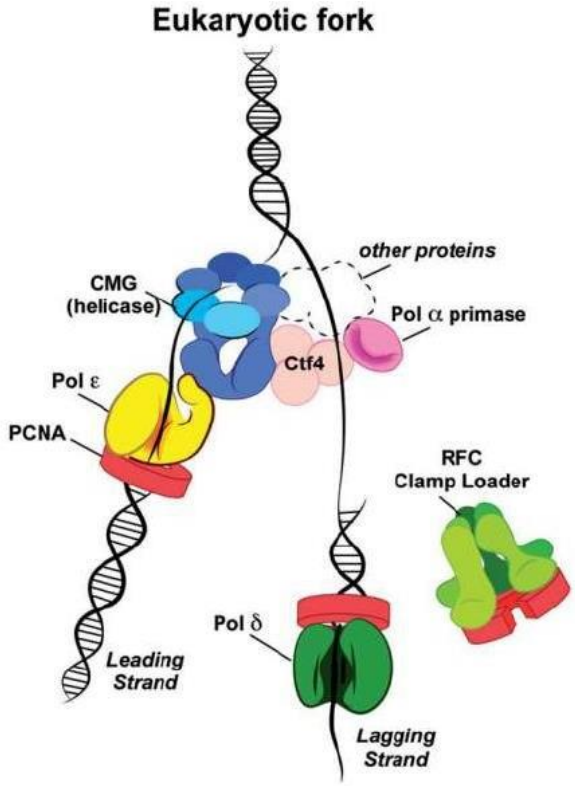

Figure 1.1: The proposed architecture of eukaryotic replisome. The helicase encircles the leading strand; the CMG helicase complex is GINS and CDC45 with Mcm2-7 to aid the unwinding. The RFC clamp loader repeatedly loads PCNA clamps onto lagging strand primers formed by pol α-primase. Next, the leading strand polymerase (Pol ε) is stabilized on DNA by Mrc1. Finally, Pol δ replicates the lagging strand [2].

Usually, when a replisome runs into DNA damage, a strand break, or a protein block, the bacterial and eukaryotic cell employ a mechanism to activate stalled DNA replication forks. Literature suggests multiple repair mechanisms, for instance, error-free and error-

prone DNA synthesis at the DNA replication fork. In addition, post-replicative repair by nucleotide excision repair or base excision repair is involved in repairing lesions not directly blocking the replication fork [3].

Significant DNA damage occurring before or during replication in eukaryotes elicits the activation of so-called checkpoint mechanisms, signalling to the cell cycle regulatory machinery, principally the CDK and DDK protein kinases, that subsequent events in the cell cycle should wait until the repair of DNA damage. The biochemistry of these varied signalling events is still being worked out, but a standard signal early in the process is the stable presence of RPA-coated ssDNA. Usually, ssDNA should be present in small quantities in the cell, but its sustained presence signals that a stalled replication fork exists due to damage or stress. Timely response to DNA damage is vital during DNA replication when the progression of the replication machinery (the replisome) over DNA lesions can result in the generation of life-threatening breaks on DNA. Consequently, some of the mechanisms that coordinate DNA repair are directly associated with the replisome. Research is focused on trying to understand how these two processes influence each other.

The signalling cascade mediated by damaged DNA during fork stalling leads to activation of checkpoint kinases, spreading the signals to several effectors that regulate various aspects of cell physiology. Factors associated with sensing and transducing the checkpoint signals generated at replication forks are highly conserved among eukaryotes. At the centre of the checkpoint signalling cascade are the phosphoinositide 3-kinases (PI3)-related mec1 and tel1 kinases. PI3-related kinases directly target the highly conserved effector kinase rad53 and chk1. Thus, they are responsible for amplifying the checkpoint signal and the phosphorylation of essential proteins that govern different aspects of cellular physiology [4].

The project's **overall objective** is to understand the relationship between DNA replication and the DNA damage response in eukaryotes using *S. cerevisiae* as a model organism. The project aimed to explore two aspects of this overarching question: the immediate response of the replisome to DNA damage; and the dynamics of the proteins that regulate DDR. With this intention, the single-molecule live-cell approach recently developed in the

Reyes lab was adopted to characterize the binding kinetics and infer the composition in the DNA replication machinery of yeast cells.

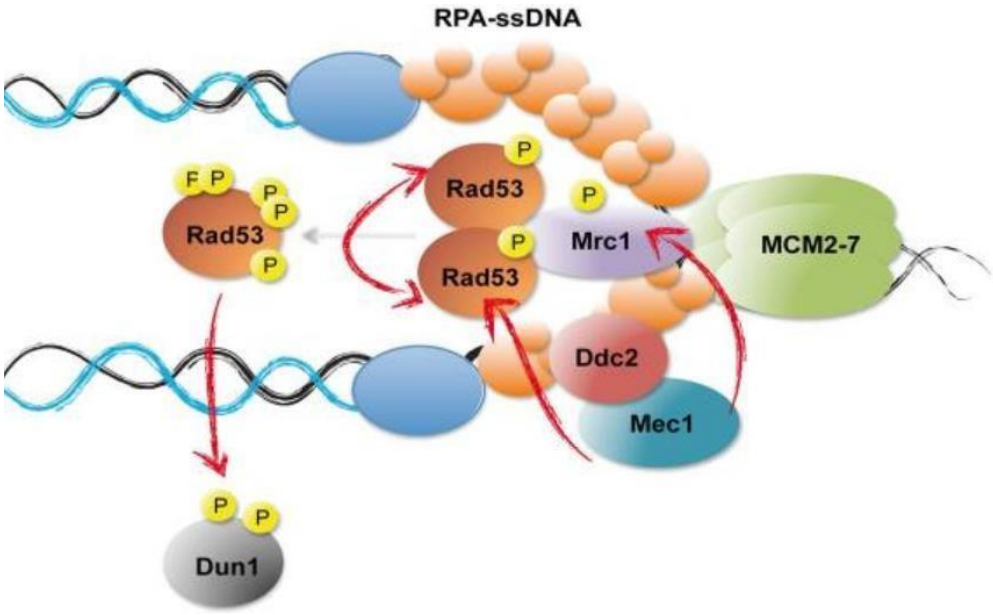

Figure 1. 2: Checkpoint activation in response to replication stress. Upon replication fork stalling, ssDNA is generated by the replicative helicase-DNA polymerases uncoupling. RPA-ssDNA mediated the recruitment of the apical checkpoint kinase Mec1 to replication forks by the action of its associated factor Ddc2. Mec1 phosphorylates fork components, including the Mrc1 transducer and the Rad53 effector kinase. Mrc1 serves as a scaffold promoting Rad53 trans-autophosphorylation events and full kinase activation. Rad53 phosphorylates and activates Dun1 effector kinase [5].

Several replisome components, including α and δ subunits of DNA polymerase and MCM helicase complexes, are direct targets of Mec1 and Rad53 phosphorylation. Furthermore, the association of replicative polymerases and helicase complex to stalled replication fork is impaired in checkpoint kinases mutants [6][7]. These observations led to the suggestion that checkpoint kinases might regulate the tethering of essential replisome components to the DNA. The loss of this tethering could be why the checkpoint mutants' inability to

resume DNA synthesis. This hypothesis led to the project's **first aim** to characterize the immediate response of replisome to DNA damage (Described in **Chapter 4**).

Recent work from our lab has shown that most core subunits in the yeast replisome, except the Pol α, which serves as a primase, are stably bound to chromatin during DNA replication. This data was used as a starting point to study the replisome after DNA damage. *The following hypothesis was that the composition and dynamics of the replisome change after cells are submitted to stress*. Various literature reports composition alteration of the replisome after blocking DNA replication that remains controversial. The single-molecule approach is more sensitive and has a better time resolution than other approaches used in the past to study this question. The dynamics of the untreated and cells treated with UV were characterized as a part of aim1 for the project.

As a **second aim,** I intend to characterize the dynamics of factors, like apical kinase and effector kinases, involved in the DNA damage response (**Chapter 4**). The DNA damage checkpoint pathways sense DNA lesions and remodel the signals into relevant biological responses. Two key factors controlling this response are the checkpoint kinase, like Mec1, and its effector kinase, like Rad53. The model is that Mec1 binds to stalled DNA replication forks and mediates the phosphorylation of multiple targets, including Rad53. Thus, the question aimed to characterize the binding dynamics of the kinases to chromatin in actively growing and stressed cells.

Numerous pieces of literature articulate the development of fluorescence microscopy. This technique has enabled us to study protein kinetics directly in the living cells, with the most common techniques being single-particle tracking (SPT), fluorescence recovery after photobleaching (FRAP), and fluorescence correlation spectroscopy (FCS). A conclusion in the literature states that the data obtained from SPT makes qualitative and quantitative interpretation much more effortless than other approaches [2].

However, various intrinsic factors constrain yeast's microscopy, like nuclear movement, thicker cell walls, and a higher endogenous fluorescence (compared to bacteria). Furthermore, the type of dye could also play a significant role in visualizing the single molecules required in the earlier stated hypothesis. Therefore, the study of these factors

in single-molecule microscopy of yeast led to the extended **third aim** of my project. In **Chapter 5,** I characterized different factors affecting the quality of the images obtained by SPT. Meanwhile, in **Chapter 6,** I study the movement of the nucleus in yeast as a factor that may impact the study of chromatin-bound proteins by single-molecule microscopy.

Before describing the results obtained in my project, I first provide a literature review focused on yeast and microscopy (**Chapter 2**) and provide details on the methods used (**Chapter 3**). I provide a summary of my work in **Chapter 7**.

Chapter 2: LITERATURE REVIEW

Yeast biology and DNA Replication

Saccharomyces cerevisiae is a species of yeast well suited as a model organism for biological research. *S. cerevisiae* is a unicellular organism of approximately 5-10 μm in diameter with a short generation time and proficient gene editing by homologous recombination. As a eukaryotic organism, its cellular complexity is closer to animal and plant cells. All these features make S. cerevisiae a good model organism to study eukaryotic cell biology.

The nucleus, one of the many membrane-bound organelles of eukaryotic cells, contains most of the cell's genetic material and has several vital functions: regulating gene expression, the transport of mRNA, separating chromosomes, and ribosome assembly. In addition, the cell replicates the DNA and ensures its correct partitioning.

DNA replication is a complex mechanism that occurs in three main stages: initiation, elongation and termination. During these steps, many proteins cooperate in carrying out this process. One of the first steps is loading the DNA helicase onto the DNA; in S. cerevisiae, this is the Mcm2-7 complex [8]. Six Mcm2-7 subunits form a structure around the DNA and move in a 3' to 5' direction separating the double-stranded DNA [9]. Two essential proteins of the replisome associated with the Mcm2-7 complex are the proteins Cdc45 and GINS that stimulate the helicase [10][11]. Next, replication protein A (RPA) binds the single-stranded DNA, stabilizing it and removing secondary structures. There are three different DNA polymerases present in the budding yeast replisome. Each of these polymerases plays a different role in DNA replication [12]. Pol ε is responsible for synthesizing the leading strand, while pol δ is associated with synthesizing the lagging strand. Proliferating cell nuclear antigen (PCNA) clamps tightly to the polymerase and serves as a processivity factor for Pol δ [13]. PCNA is loaded onto the DNA by the clamp-loaded Replication Factor C (RFC) [14]. Pol α has a primase subunit and can generate

and extend RNA primers but is not suited for extensive DNA synthesis [15]. Ctf4 connects Pol α to the helicase [16], but the function of this coupling is still unknown.

DNA stress and DNA damage response

When a cell encounters stress, it initiates a repair mechanism to handle the damage or stress. Various literature indicates that eukaryotic cells respond to DNA damage and replication blocks by delaying cell cycle progression through a surveillance mechanism known as the DNA damage checkpoint, providing the time to restore the correct [63]. Furthermore, this DDR is an evolutionarily conserved process [58]. When replication fork stalls, a signalling cascade mediated by damaged DNA leads to activation of checkpoint kinases, spreading the signals to several effectors that regulate various aspects of cell physiology. Factors involved in sensing and transducing the checkpoint signals generated at replication forks are highly conserved among eukaryotes. At the centre of the checkpoint signalling cascade are the phosphoinositide 3-kinases (PI3)-related mec1 and tel1 kinases. PI3-related kinases directly target the highly conserved effector kinase rad53 and chk1. Thus, they are responsible for amplifying the checkpoint signal and the phosphorylation of essential proteins that attune various prospects of cellular physiology [4].

Several replisome components, including DNA polymerase α and δ subunits, as well as MCM 2-7 helicase complexes, are direct targets of Mec1 and Rad53 phosphorylation and the association of replicative polymerases and helicase complex to stalled replication fork is impaired in checkpoint kinases mutants [6][7]. These observations suggested that checkpoint kinases might regulate the tethering of essential replisome components to the DNA. The loss of this tethering could be why the checkpoint mutants' inability to resume DNA synthesis. This hypothesis led to the project's first aim to characterize the immediate response of replisome to DNA damage.

Various literature describes the induction as conferred by reduced transcription of histone genes and globally decreased DNA nucleosome occupancy [58]. This globally altered chromatin structure increased the expression of genes encoding enzymes of the

tricarboxylic acid cycle, electron transport chain, oxidative phosphorylation, elevated oxygen consumption, and ATP synthesis [58]. During the S phase or after DNA damage, Dun1p phosphorylates and induces degradation of Sml1p, a protein that binds and inhibits the Rnr1p subunit [59][60][61][62]. The researchers describe a model for the role of checkpoint kinases involved in DDR, as shown in figure 2.1 below. The figure also demonstrates the role of RNR in the synthesis of dNTPs to handle the DNA damage during DNA damage response.

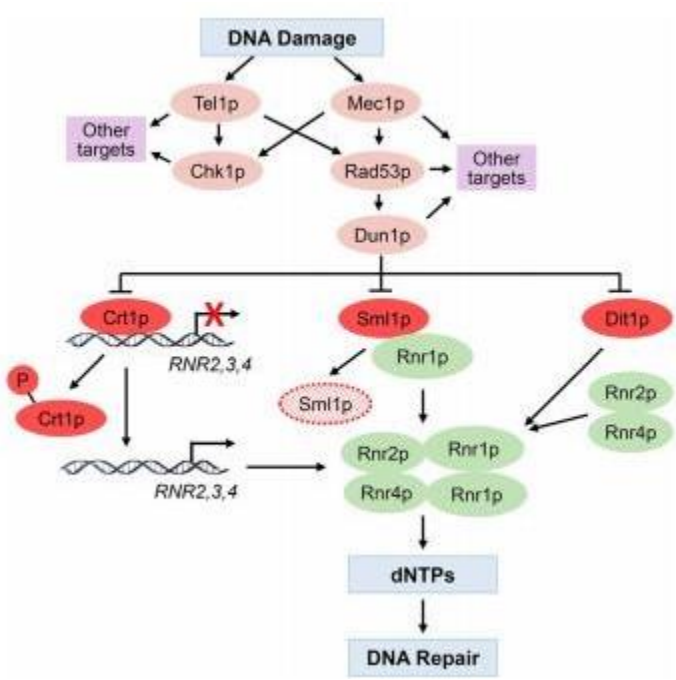

Figure 2.1: Model depicting the role of checkpoint kinases in DDR, the RNR regulation, and synthesis of dNTPs during DDR. DNA damage activates the cascade of checkpoint kinases Mec1p, Rad53p, and Dun1p. Dun1p phosphorylates and down-regulates three negative regulators of the RNR complex: Crt1p, Sml1p, and Dif1p. Crt1p is a transcriptional repressor recruited to the RNR2, RNR3, and RNR4 genes. Phosphorylation of Crt1p derepresses RNR2, RNR3, and RNR4 genes by inducing dissociation of Crt1p from the corresponding promoters.

Sml1p binds Rnr1p and inhibits RNR activity. Sml1p phosphorylation promotes its ubiquitylation and degradation by the 26S proteasome. Dif1p regulates nucleocytosolic distribution of Rnr2p and Rnr4p. Dun1p-mediated phosphorylation of Dif1p leads to redistribution of Rnr2p and Rnr4p from the nucleus to the cytoplasm, where Rnr1p resides,

resulting in the assembly of the active RNR complex. The cumulative effect of Dun1p activation is increased RNR assembly and activity and increased synthesis of dNTPs [58].

The cells must be aware of the damage, and of when DNA repair is completed, to terminate the checkpoint response and resume cell cycle progression [63]. Repair of DNA damage might restore normal cell cycle progression, and/or active mechanisms might be required to shut off the checkpoint. [63].

Importance of the study of DDR

DDR is responsible for maintaining the integrity of the DNA replication. The role of DNA repair in the initiation, promotion, and progression of malignancy suggests that deficiencies in DNA repair genes confer an increased cancer risk. Mutations in replisome subunits are linked to developmental abnormalities, deficiencies of the immune and endocrine systems and predisposition to tumour formation [42][43]. Concisely, failure of DNA repair or checkpoint controls can lead to cell lethality, mutations, genome instability and cancer [63].

Mutations in DDR factors are linked to many different diseases, including neurological defects, infertility, immunological defects and premature ageing. DDR is also implicated at all stages of cancer [44]. Understanding the relationship between DNA replication and DNA damage will likely benefit the prevention and treatment of these diseases [45].

How to study DDR in live cells?

Single-molecule experiments have become an important tool to study molecular dynamics. Over the years, microscopy techniques have evolved to improve the signal-to-noise ratio, resulting in clearer data. In addition, the use of genetically encoded fluorescent tags facilitates the study of various proteins of interest [18]. The use of the Total Internal Reflection Fluorescence (TIRF) microscopy technique, where only the

surface close to the coverslip was exposed to excitation light by an evanescent wave, helped to improve the signal-to-noise ratio. The evanescent wave occurs if the light is internal reflected at the interface of the oil and the aqueous solution of the sample hence the name total internal reflection microscopy. The oil has a higher refractive index and, past a certain critical angle, reflects the light into the oil; Snell's law governs this behaviour. When using TIRF, you can only excite a thin region of the sample adjacent to the coverslip [19]. Since only a fraction of the fluorophores is excited, there is a low degree of background fluorescence. Since the replisome proteins are in the nucleus - typically deeper in the cell than 200nm that can be observed by TIRF - it is impossible to use TIRF microscopy to study them. Instead, researchers use a technique derived from TIRF called Highly Inclined and Laminated Optical (HILO) sheet microscopy [46]. To increase the signal-to-noise ratio, the illuminating beam was inclined to minimize the area of illumination. The inclination of the beam by refraction leads it to hit the sample as a thin optical sheet. This sheet always passes through the center of the sample, so using this technique, it is possible to image the components of the replisome. In combination with photoactivatable fluorophores, this can be a powerful tool to study molecule dynamics.

Photoactivatable fluorophores are fluorophores that photons can activate with a wavelength of 405 nanometers. By activating only a small number of proteins, you are more easily able to detect single molecules. The photoactivatable fluorescent proteins help measure the bound times of specific proteins of the replisome [20].

(a)

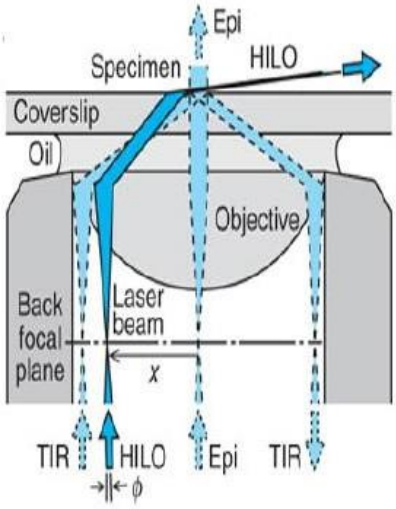

(b)

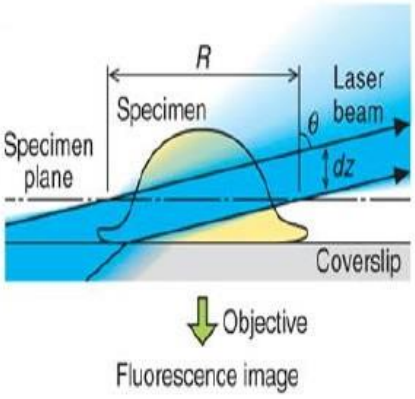

Figure 2.2: (a) Schematic overview of the light traces while using TIRF and HILO microscopy techniques (b) Schematic overview of the thin light sheet passing through a sample [17]

Generating a protein with a fluorescent protein tag or performing immunofluorescence are common ways to do this. A lesser-known way to tag a specific protein is by combining HaloTag and HaloTag ligands [21]. The first thing to take care of is the fusion of HaloTag and the protein of interest. Next, a synthetic ligand needs to bind to the HaloTag covalently. For microscopy purposes, the most useful HaloTag ligands are the various types of fluorescent dyes as listed in Appendix IV. This is a useful tool in biology because sometimes it is necessary to image multiple proteins at the same time, e.g. study co-localizations. When fusing a protein with HaloTag, a fluorescent dye can be chosen so it does not interfere with the excitation-absorption spectra of the other protein of interest [21]. This is a clear advantage because this HaloTag fused protein strain can be combined with more strains than a regular fluorescent protein strain. Figure 2.3 below depicts the interaction of HaloTag and how it helps the dye bond with the protein of interest in microscopy.

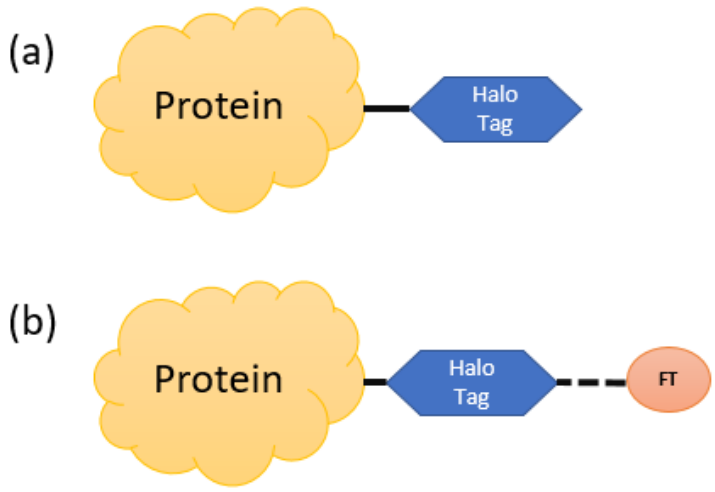

Figure 2.3: HaloTag Fusion with the protein of interest (a) shows the first step of the process: fusion of the protein of interest (yellow) with a HaloTag (blue). (b) shows the next step:

addition of a synthetic ligand, here fluorescent HaloTag Ligand (Fluorescent Tag in orange), to the HaloTag by a covalent bond (black dotted line).

There is a wide range of other fluorescent dyes available, all with different fluorescence excitation absorption spectra. This is a valuable tool in biology because sometimes it is necessary to image multiple proteins simultaneously, e.g. study co-localizations. Furthermore, a fluorescent dye is such that it does not interfere with the excitation-absorption spectra of the protein other than the protein of interest, that is, HaloTag fused protein and PCNA with mNG labelling [51]. The excitation coefficient, a measure of the amount of photon that can be absorbed, and quantum yield, the ratio of an absorbed photon over emitted photons, should be as high as possible. The product of these measures is called brightness [51]. The fluorescent dyes should be selected based on some of these criteria.

Factors affecting Single-Molecule Microscopy in live yeast

Despite the significant characterization of both prokaryotic and eukaryotic replication proteins in vitro, the limitation of study DNA replication dynamics in live cells is a longstanding biological and technical obstacle [20]. Various biochemical studies performed at the cell population level led to many advances in identifying and characterizing the replisome. However, population averaging is limited in its capacity to capture the biologically relevant variation in replication dynamics across cells and protein subpopulations' distinct behaviour. Furthermore, established approaches lack the spatial and temporal resolution to fully characterize the dynamics of DNA replication within the context of a single living cell. Decades of research have contributed to our knowledge of replication proteins and the global pattern of DNA replication, primarily through biochemical and structural approaches [20][32]. Still, many questions regarding the mechanical features, dynamic behaviour and organization of the replisome remain open.

The development of single-molecule microscopy techniques has provided new and exciting opportunities to study the behaviour of single molecules *in* vivo, overcoming the

diffraction limit of light (~250 nm) found in conventional fluorescence microscopy [31][32]. However, these methods rely on the illumination of a small fraction of all fluorescently labelled molecules in a narrow plane near the coverslip's surface to improve the signal-to-noise ratio during imaging. This configuration presents additional challenges for study in budding yeast cells, which have a spherical shape and an approximate diameter of 5 µm, and therefore require a greater distance of light penetration to visualize molecules in the nucleus [33]. Thus, single-molecule studies have been limited in yeast despite their powerful potential to elucidate the dynamics of fundamental biological processes in the cellular context. Being a eukaryotic model, yeast has certain limitations when it comes to microscopy, like the thick cell wall, which causes hindrance when illuminated with a laser beam [57].

Similarly, the selection of fluorescent protein and dye has always been challenging [56][57]. If looking at a single fluorophore, a suitable filter that can collect most light is recruited for the purpose. Whereas while working with multiple fluorophores, a filter with a narrow band of excitation and absorption spectra is used to avoid overlapping [56]. Furthermore, the viability of cells can be affected by the growth conditions [57]. These need to be taken into consideration while working with yeast microscopy.

Bioinformatics Analysis of proteins involved in DDR

Lately, many researchers have reached out to bioinformatics or structural analysis if a certain known technique does not work the way it was expected to. For instance, genome sequencing reveals hundreds to thousands of somatic mutations in each tumour. Not all cancer mutations provide a selective (or "driving") advantage to cancer cells. Many mutations are so-called "passengers" because their impact on protein function is either insignificant or the affected protein is not important for tumour progression [28]. The mutations could alter the stability or the functionality of the genome, resulting in some unexpected outcomes. The International Cancer Genome Consortium (ICGC) aims to catalogue genomic abnormalities in tumours from 50 different cancer types. Certain researchers have compiled the result of discussions within the ICGC on how to address the challenge of identifying mutations [28].

Genetic instability is a characteristic of most cancers that may play a critical role in driving the accumulation of genetic changes that underlie tumorigenesis. Various bioinformatic procedures have been developed using genome-wide functional genomics screens to identify and prioritize candidate suppressing genes [29]. The number of known suppressors was increased from 75 to 110 by testing 87 predicted genes, which identified unanticipated pathways in this process [28][29]. The bioinformatics analysis explicitly deals with the lack of concordance among high-throughput datasets to increase the reliability of phenotypic predictions.

Various literature suggests that the mec1 strain is more viable with N-terminal fusion [64]. The apical kinase tends to develop variants that are deleterious when transformed using C-terminal transformation. Hence the use of CRISPR- Cas9 technology will provide a marker-free integration of HaloTag to the N terminal of the mentioned proteins.

CRISPR-Cas9 for N-terminal fusion of HaloTag

The CRISPR-Cas9 technology is an essential tool for genome editing because the Cas9 endonuclease can induce targeted DNA double-strand breaks. A sgRNA and the guide sequence together control the DNA break targeting. A sgRNA is a chimeric RNA segment containing a structural component essential for the cas9 binding. The guide sequence is a 20mer segment that hybridizes to the genomic DNA target [23]. Previous studies have demonstrated that using CRISPR-Cas9 technology makes marker-free genome editing in S. cerevisiae more efficient. However, inserting the guide sequence into yeast sgRNA vector usually requires cloning procedures that are time-consuming, complicated and expensive. Therefore, developing these techniques to simplify the sgRNA vector with internal restriction enzyme sites allows fast and directed cloning of the guide sequence. Multiple literature works suggest using various adaptable sets of vectors for cloning in yeast by using distinctive selectable markers [22]. Literature indicates that the Cas9-sgRNA vector and the URA3 selectable marker would prove advantageous for yeast genome editing considering the cas9 machinery can be easily removed by counter-selection using 5-FOA following successful genome editing [22][23][24]. To accelerate

the use of CRISPR-Cas9 technology in yeast genome editing, there is a need for new vectors that can simplify and establish the technical steps required for guide sequence cloning [24].

CRISPR-Cas9 technology was employed for the N-terminal fusion strains as described earlier. In the system used, the guide RNA (gRNA) and the Cas9 gene are expressed from the same plasmid. Therefore, the first step is to clone a gRNA targeting the gene (region) of interest into a plasmid expressing Cas9 [22]. The yeast is then transformed with the resulting plasmid, inducing a double-strand break at the targeted site. Therefore, if the break is not repaired, all cells expressing this plasmid will die. This repair is guided by co-transforming a repair oligo (usually a double-stranded although single-stranded oligos should work) or a repair PCR fragment. This repair DNA is designed to introduce the desired mutation during the recombination/repair [22].

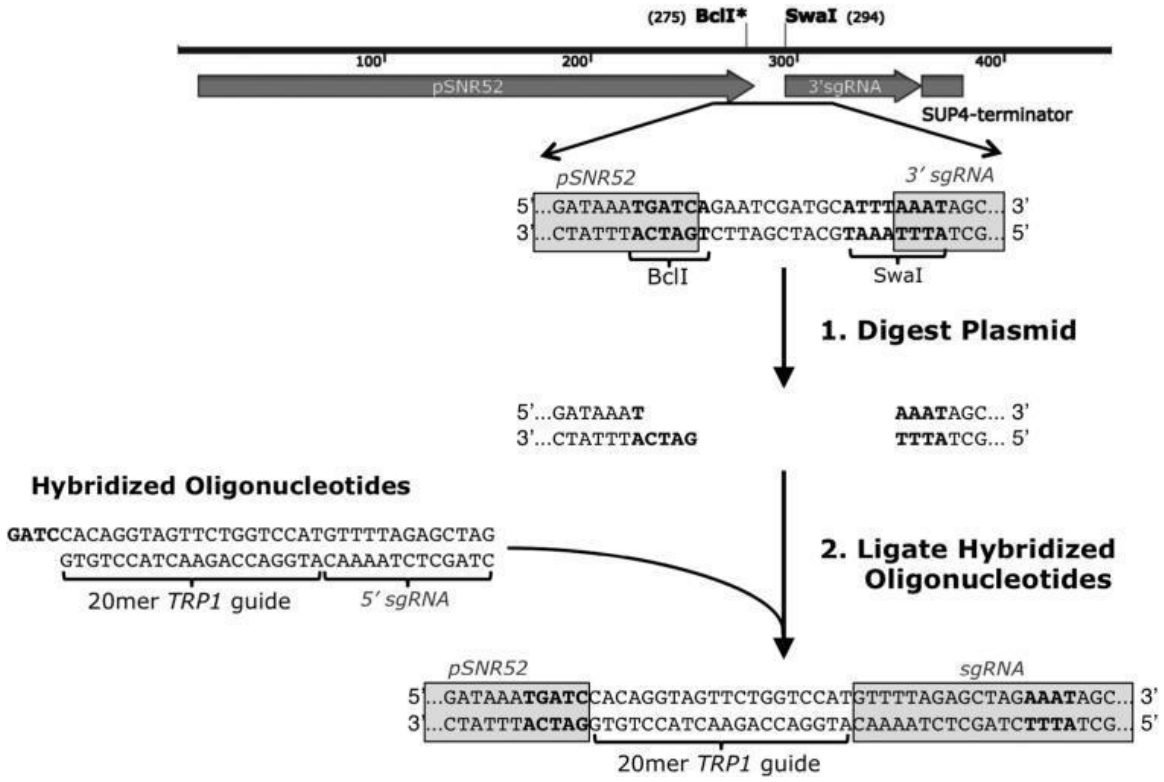

Figure 2.4: CRISPR-Cas9 technique: Design of new guide RNA expression cassette for rapid cloning of 20mer guide sequences. Unique BclI and SwaI sites enable efficient cloning of any 20mer guide RNA targeting sequence into the single guide RNA (sgRNA) expression

cassette. A plasmid with the guide RNA expression cassette is linearized by digestion with BclI and SwaI enzymes. Oligonucleotides are designed to contain a compatible GATC overhang, a 20mer guide sequence, and the 5' end of the structural segment of the sgRNA. The hybridized oligonucleotides are ligated into the digested plasmid, yielding the final complete sgRNA expression cassette. The asterisk indicates that BclI cutting is blocked by Dam methylation [22].

For Cas9 to cut DNA, a protospacer-adjacent motif (PAM) must be present in the genomic DNA immediately 3’ to the target site. PAM sequences are either NGG or NAG trinucleotides, the latter being less efficient. The presence of PAM sequences in the target sequence will therefore guide the design of the gRNA [22][23]. In addition to introducing the mutation of interest, the repair DNA will introduce a second mutation that will destroy the PAM, preventing Cas9 from entering another round of cutting after the repair process. This mutation has to be silent, representing the main limitation in choosing the appropriate gRNA, as many gRNA will be associated with PAM sequences that cannot be destroyed without introducing a change in amino acid in your protein. When everything works as expected, all clones should be positive since the expression of Cas9 is suicidal unless the cut is repaired. However, we found that secondary mutations are often introduced, so clones should be sequenced carefully. Once a positive clone is identified, it is recommended to eject the plasmid, which is quickly done since cells having lost the plasmid rapidly take over a liquid culture grown in the absence of selection [22].

Nuclear movement in yeast

One of the interesting factors to be considered while working with the nucleus of budding yeast is its positioning and movement in the cellular environment. In interphase *S. pombe* cells, the nucleus is positioned in the middle of the cylindrical cell in an active microtubule (MT)-dependent process. Literature suggests that interphase MTs are organized in three to four antiparallel MT bundles arranged along the long axis of the cell. The MT bundles are organized from medial MT-organizing centers that may function as nuclear attachment sites. Instead of functioning as tracks, MTs may function in nuclear positioning by exerting pushing forces on the nucleus through MT polymerization. The

movement of the nucleus in fission yeast is recorded to be constrained and controlled by microtubules. A scarce systematic description of the positioning of the nucleus during the cell cycle has been done in budding yeast that quantifies its movement. DNA replication takes place in the nucleus. Therefore it is important to correct for nuclear drift when generating single-molecule tracks of replisome components [37].

In contrast to the lack of information on the dynamics of the nucleus, research has been carried out to study the effect of stress on chromatin material. Researchers did not notice any significant change in the movement when treated with nocodazole, but on treating the cell with latA, the chromatin movement was majorly reduced [65]. To test for potential participation of the cytoskeleton in the control of nuclear movement, the cells are treated with nocodazole to inhibit microtubule and with latrunculin A to inhibit actin. Studies from several species show that the baseline movement of chromatin within an interphase nucleus occurs with a subdiffusive character. This means that chromatin roams within a restricted volume that is significantly smaller than the volume of the nucleus. Internal forces, such as nucleosome–nucleosome contacts or sister cohesion, constrain free diffusion. The mobility of tagged loci was influenced by ATP levels or DNA interaction with fixed elements at the nuclear envelope. This could also be provoked by a forced loss of nucleosomes from DNA through mutation or histone shutoff [65].

Mathematical models for analysis

The analysis of data plays a major role in understanding or interpreting it. Sometimes when unexpected results are encountered, modelling these data can reveal unanticipated outcomes. Under similar conditions, SIFT (Sorting Intolerant From Tolerant) scoring has been reviewed by many researchers. Literature indicates that SIFT scoring can distinguish between functionally neutral and deleterious amino acid change [52].

Various mathematical models are involved in analyzing the data collected for various experiments. One of the techniques mentioned in multiple works of literature is the signal-to-noise ratio, and it means squared error to determine the quality of data

collected. SNR is the relation of the desired information to the undesired information or the power of the background noise. The MATLAB function to calculate the SNR is a powerful tool of signal processing library that creates a small mask and runs it over the entire array of pixels for all the consecutive frames [50]. The masked region is checked for the desired signal that is the single-molecule spots for our experiments, using the Gaussian fit, as would be used by the Trackmate plugin of Fiji for track segmentation. The desired signal is compared to the unwanted background. This comparison gives an estimate or possibility of a disruptive signal in the data that might interfere with legitimate data [50]. And for each mask mean squared error is calculated. MSE is the mean of squared pixel difference of consequent frames to determine how close they are [49]. The squaring is required to eliminate any negative values while taking the difference. The lower the average squared difference, the better the image since there is not much deviation to be noticed in the background. This is the measure to check how consistent or noise-free the background is.

Literature suggests that the nucleus has sub-diffusive behaviour owing to its viscoelastic fluid environment in the cytoplasm, with other membrane-bound organelles and proteins that might hinder its free movement. The mean square displacement was calculated by

$$MSD = \big(r(t) - r(0)\big)^2$$

Where the r0 vector was shifted to gain more data out of the tracks. An average was taken over all the individual tracks to get a final MSD curve. The r(t) vector is calculated using the x and y coordinates as calculated by MATLAB tracking script by the formula

$$r(t) = [(x2 - x1)^2 + (y2 - y1)^2]^{\frac{1}{2}}$$

Anomalous diffusion is a diffusion phenomenon in which the diffusive process has a non-linear relation with time [39]. When analyzing the microscopy data, an interesting parameter to resolve is the diffusion coefficient and its dependence on the α coefficient. These coefficients are very informative about the movement and characteristics of the different molecules. The diffusion coefficient will study the diffusion concerning a mean

trajectory x(t), where this mean trajectory is the solution to the deterministic equation of motion. Since the diffusion coefficient is the first derivative of the mean square displacement with respect to time, it will depart from its theoretical value [66]. But the α coefficient characterizes the diffusion of the molecule [41][66].

For instance, if α = 1, the process is described by typical diffusion (blue in Figure 2.5). If α > 1, the diffusion process is termed superdiffusion (green in Figure 2.5). An example of a cellular process that has this behaviour is the movement of cargo by a motor protein [40]. When α < 1, the movement behaves subdiffusively (red in Figure 2.5), chromosomal loci movement has been shown to be subdiffusive [41].

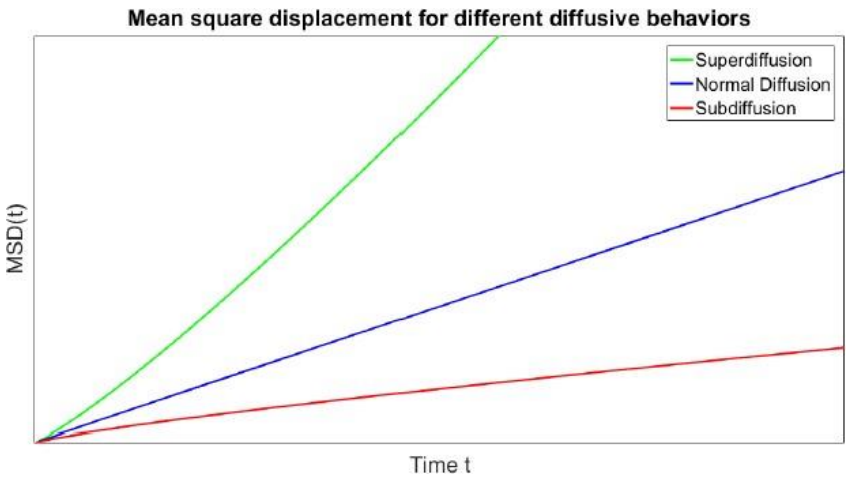

Figure 2.5: The mean square displacement is proportional differently to time for different types of diffusion. MSDs of superdiffusion, normal diffusion and subdiffusion are shown in green, blue and red, respectively (modified from [40][41])

Anomalous diffusion can describe more complex physical processes which cannot be described by typical diffusion. Some models represent anomalous diffusion. One of them is a generalization of Brownian motion, fractional Brownian motion. In fractional Brownian motion, the increments do not have to be solely independent. In a biological context, it makes sense that anomalous diffusion is observed. When looking at the

movement of certain components in cells, it could be that they are embedded in a protein polymer network, that they are mechanically coupled or just the inability to freely roam around because they are being blocked by the other cellular components. This would mean that each increment is not independent anymore, thus corresponding to the fractional Brownian motion model.

The literature proposes that anomalous diffusion found in SPT data results from weak and transient interactions with dynamic nuclear substructures and that SPT data analysis would benefit from a better description of such structures [55].

Chapter 3: MATERIALS AND METHODOLOGY

Plasmid Construction

The plasmids used in this study were maintained in *E. coli* and were extracted by growing in LB then using the Presto Mini Plasmid Kit (Geneaid). Cell pellets are harvested from this bacterial culture. Cell pellets are resuspended in 200 µl PD1 buffer with RNase A. 200 µl PD2 buffer was added to the mixture gently and avoid shearing the genomic DNA. The mixture is set to rest at room temperature for about 2-5 minutes to get homogenous consistency. 300 µl of PD3 buffer is added and mixed gently to neutralize the mixture. The supernatant from the centrifuged mixture is transferred to a PDH column without disturbing the precipitate. The flow-through is discarded, and 400 µl of W1 buffer is added to the PDH column. The flow-through is again discarded. 600 µl of wash buffer with absolute ethanol is added to the PDH column. Flow-through is again discarded, and the column matrix is left at room temperature to dry. 50 µl of elution buffer is added to the center of this column matrix and is left to be absorbed entirely for 2 minutes. Then, purified DNA is eluted by centrifuging the column at room temperature.

Primer Designing: C Terminal

The DNA sequence (with +/- 1kb, also known as flanking genome) for the gene of interest is obtained from the yeast genome database (https://www.yeastgenome.org). The transformation and screening primer for our gene of interest is designed using serial-cloner (open-source software). The gene sequence is loaded into the software to identify the forward and reverse primer. The gene-specific forward primer is selected by identifying 40bp before the stop codon (excluding the stop codon). The reverse primer is selected by identifying 40bp after the stop codon (excluding the stop codon). The forward screening primer is the 18-20bp fragment followed by the segment of 150-200bp before

the forward primer insertion. Similarly, the 18-20bp reverse screening primer is followed by a segment of 150-200bp after the reverse insertion primer.

Primer Designing: N Terminal

The predesigned oligos for cloning a gRNA into pML104 and pMLl107 were obtained from an online tool for guide sequence cloning by Wyrick lab. (http://wyrickbioinfo2.smb.wsu.edu/crispr.html) The repair oligos should contain the desired mutations (including one destroying the PAM) and at least 40 bases on each side of the mutation sites. We usually design oligos for both strands. If the distance between the PAM and the mutation is too long, oligos may not provide enough homology on each side for efficient recombination. In such a case, ordering two convergent oligos (about 70nt each) overlapping by about 15-20nt could be considered.

Strain Construction/Transformation C Terminal

The strains used in this study are all from BY4743 background. The plasmid used in this study are maintained in *E. coli* and are extracted by growing in LB then using the Presto Mini Plasmid Kit(Geneaid) [35].

All PCRs are performed using the Q5 enzyme. PCR mixture is in the volume of 50 µl with water, 3% DMSO, the reaction buffer, 2.5 mM of each dNTP, 0.2 µM of each primer, either 1ng of plasmid DNA (for insertions) or 1 µl of genomic DNA (for screening insertions), and 0.5 µl of polymerase [35].

Fluorescent fusions are made by PCR amplification from pSJW01 using their corresponding primers. PCR products are transformed into wild-type diploid BY4743. A single colony was grown at 30°C in 5 ml yeast peptone dextrose (YPD) overnight. It is later diluted to 0.1 OD in 10ml of YPD [2]. Cells were taken at OD of 0.5-0.6 and centrifuged at 4000 rpm for 5 min. It is then washed twice with 25 ml of sterile deionized water and once with 1ml of 100mM lithium acetate. Cell pellets are later resuspended in a mixture with the following order and concentration. It has 240 µl of 50% PEG and 50 µl

of salmon sperm DNA, which is thawed at 95°C for 5min then incubated on ice for at least 10min. The mixture also contains 50 µl of the PCR product and 36 µl of 1M lithium acetate. It is thoroughly mixed by pipetting and incubated on a rotator at 25°C for 45min, followed by 30min heat shock at 42°C. The cell pellets are washed in 500 µl of sterile water, then resuspended in 200 µl of YPD and plated on YPD agar. After growing at 30°C overnight, the cell lawn is replica-plated onto selective YPD agar, either with 100 µl/ml cloNAT (Werner) for mNeonGreen or 200 µl/ml Hygromycin B (Life Technologies) for HaloTag. The transformants are lastly screened for the presence of an insert by PCR using the indicated screening primers. The confirmed clones are later sporulated [2][35].

In order to sporulate the confirmed clones, 750 µl of a YPD overnight culture is washed four times with 1 ml sterile deionized water and washing once with 1 ml of potassium acetate sporulation medium (KAc). It is finally resuspended in 2 ml of KAc and incubating at 25°C with shaking. After 7-10 days, the sporulating cultures are checked using microscopy for the appearance of numerous tetrads, then 750 µl is taken and washed three times in sterile water before final resuspension in 1ml water and storage at 4°C. For dissection, 45 µl of spores is treated with 5 µl of zymolase for 10 min; then, tetrads are dissected on YPD plates to isolate haploids with the tagged fusion. Genomic DNA is separated from the haploid by vortexing the cells in the presence of zirconia/silica beads, followed by phenol extraction and ethanol precipitation. The insertion site is amplified using the same screening primers as above, and the PCR product is sequenced to confirm that the tag and linker are both mutation-free. The HaloTag haploids are lastly combined with PCNA-mNeonGreen (from YTB31) by mating [35].

Strain Construction: CRISPR-Cas9

In the case of CRISPR-Cas9 technology, 1.5µl of the two repair oligos of 10µM concentration, with 5µl of 10X KOD buffer, 3µl of MgSO4, 5 µl of 2mM dNTPs, 1µl of KOD and 33µl of water, giving a 50µl of the reaction mixture that is used in PCR. This reaction generates a 120bp long dsDNA fragment that will be later used for repair [22]. The extended product is then purified using the Qiagen PCR purification clean-up kit and quantified on Nanodrop [22].

Next, we need to anneal the gRNA with the repair oligos. 25 µl of a mixture containing each oligo is suspended in 10mM Tris pH8.0 (or water) at 100µM, along with 37.5 µl of each gRNA oligo. The mixture was thoroughly mixed by pipetting followed by heat shock at 95°C for 5min. It is then transferred into a 70°C heat block, and when it reaches room temperature, the mixture is allowed to rest at 4C overnight [22].

These annealed gRNA oligos are cloned into the two digested plasmids of pML107 and pML107 using 10x NEB 3.1 buffer and SwaI. These plasmids are incubated overnight at room temperature. Later, 1µL BclI is added to the plasmids, followed by a 2-hour incubation at 50C. Finally, the plasmids are gel-purified and are ready to be used in ligation reaction along with 0.65pmol (i.e. 0.5µL of 1:29) of annealed gRNA oligos, 2µL of 5x ligation buffer, 0.5µl of Ligase H.C. and water to make a reaction mixture of 10µL incubated at 16C for 3 hours. Everything is transformed into DH5α. Plate everything on a single LBA plate [22]. The colonies generated are screened by PCR using plasmid targeting the vector and the Oligo 2 from the gRNA. Positive clones will develop a 350bp amplification.

The positive colonies are transformed into yeast. 400ng of the plasmid is transformed with repair DNA. The repaired DNA can be 300pmol of ds repair oligos, 300pmol of ss repair oligo, 400ng of PCR-extended oligos or 1µg of repair PCR product. Transformation is done using the TRAFO method. Plate 1%, 10% and 90% on Ura- (if cloned into pML104) or Leu- plates (if cloned into pML107). The colonies are selected colonies, and DNA extracts are prepared and are amplified over the target region by PCR using KOD polymerase. Finally, the PCR fragments are sent for sequencing. Lastly, to eject the plasmid. The positive clones are grown in YPD liquid for several generations; serial dilutions and plating on YPD, YNB complete or any appropriate plate that does not select for the CRISPR plasmid is required [22]. If pML104 is used, it can be plated on FOA. The final clones that do not grow on Leu- or Ura- plates are re-sequenced.

Sample Preparation for Single-Molecule Microscopy

A single colony from a YPD plate is placed in a 5ml synthetic complete (SC) medium and grown with shaking at 30°C for around 5–6 hours. This culture is diluted by transferring 50µl into 5ml of fresh or filtered SC and grown overnight at 30°C. The overnight culture is diluted to 0.15 the next day and grown until the OD reaches 0.30. Next, 1ml of this culture is spun down for 1 min at 7000 RPM. The pellet is resuspended in 500µl of fresh SC, and a Janelia Farms dye, as listed in Appendix IV, is added to the culture for a final dye concentration of 50 nM. The culture of Histone H3 with halo tag fusion, a concentration of 10nM, is used to compensate for the higher copy number. The culture is placed in a thermomixer at 30°C and 500 RPM for 40 min. After incubation, the unbound dye is washed away by three wash cycles using SC. After the final wash step, the pellet is resuspended in 20µl of SC, and 3-5µl of the culture is placed on a microscope slide prepared either with agarose and gene frame or on coverslip prepared using Concanavalin A.

The agarose pad is made by taking a 2% agarose Optiprep(Sigma) mixture that is prepared with 0.02g of agarose in 1 ml Optiprep. It is heated to 90°C and mixing 500 µl with 500µl 2×SC, producing a 1% agarose 30% Optiprep SC mixture. Approximately 140µl of this mixture is placed within the Gene Frame. The excess mixture is removed with a KimWipe. Before imaging, it is recommended to wait for about 15min to let any unbound dye be released. Another experiment to study the effect of Optiprep on the data quality required preparing the agarose pad with filtered SC instead of Optiprep with agarose.

For rapid mounting and imaging of yeast, 20 µl of 0.1% Concanavalin A, commonly known as ConA, is pipetted on a high-resolution clean glass coverslip and incubated for 2-3 min. The coverslip is washed twice with distilled water, and 10 µl of prepared culture is spread onto the ConA-coated coverslip. The coverslip is left to incubate for 2 mins and later washed twice using SC medium. Finally, the coverslip is mounted on a microscope slide, and excess SC is wiped using KimWipe [36].

For the experiments to study DDR, the mixture, after being placed onto the gene frame, is exposed to UV radiation for 1-5 minutes with a pulse of 5 J/m^2. The treatment is

supposed to deplete the dNTP pool, leading to ssDNA accumulation, hence initiating DNA damage response [25].

Cleaning Cover Slips

Coverslips are cleaned with the following steps [35]:

a. place in 2% VersaClean detergent solution overnight;
b. wash with MilliQ water 3×;
c. sonicate in acetone for 30 min;
d. wash with MilliQ water 3×;
e. place in methanol and flame coverslips using Bunsen burner;
f. place in Plasma Etch plasma oven for 10 min.

Single-Molecule Microscopy

Microscopy is performed at room temperature on a Leica DMi8 inverted microscope with a Roper Scientific iLasV2 (capable of ring total internal reflection fluorescence (TIRF) and an Andor iXON Ultra EMCCD camera. An Andor ILE combiner is used, and the maximum power from the optical fibre was 100 mW for the 405 nm wavelength and 150 mW for the 488 nm and 561 nm wavelengths [35].

Single-particle photoactivated localization microscopy (sptPALM) experiments are performed by activating molecules with low power (0.5-2% in software) 405nm light to photoactivate around one molecule/cell, followed by stroboscopic, long-exposure (500ms) illumination with 561nm light (5-7% in software) to image primarily bound molecules.

The data acquisition to study the effect of nuclear movement employed different software and parameters for microscopy. A drop of yeast cells is put on a 1% low fluorescence agarose pad to image yeast strains. Clean coverslips are used to reduce background fluorescence. Imaging of the nuclei is performed with a 100x objective lens; fluorescent proteins are excited for 50ms by light from a lamp light source. The nuclei are

imaged for 25min with a framerate of 1 frame per second. SPC42-HaloTag-PA-JF549 is performed with the 60x objective lens and is excited by light from the iChrome Multi-Laser Engine. A short pulse of 30ms of the 20% 405nm wavelength laser is used for activation. The dye is excited by the 561nm wavelength laser for 300ms. H2B-GFP strains were imaged for 500 frames with an activation event every 50 frames.

The cells are treated with nocodazole or latrunculinA before imaging them under a microscope to understand the factors that affect the nuclear movement. In addition, the H2B-GFP cells are fixed before imaging under the microscope to test the precision of the localization script.

Analysis of Data

1. SIFT Scoring: It is a program that predicts whether an amino acid substitution affects protein function so that users can prioritize substitutions for further study by using sequence homology for the prediction. It presumes that important amino acids will be conserved in the protein family, and so changes at well-conserved positions tend to be predicted as deleterious. If the sequences used for prediction are closely related, many positions will appear conserved, and SIFT will predict most substitutions to affect protein function. To alert the user to these situations, SIFT calculates the median conservation value, which measures the diversity of the sequences in the alignment. Conservation, as measured by information content [53], is calculated for each position in the alignment, and the median of these values is obtained. Predictions based on sequence alignments with higher median conservation values are less diverse and will have a higher false-positive error. When the sequences in the alignment used for prediction are closely related, many positions appear conserved and important for function. Even if there are few homologous sequences available, SIFT performs better than predicting non-conservative amino acid substitutions as deleterious, where non-conservative changes are defined as having negative scores in an amino acid substitution scoring matrix. When it is not feasible to conduct experiments on all substitutions,

SIFT and other similar prediction tools [54] may be useful in prioritizing which changes affect protein function and may contribute to phenotypic differences

2. Tracking: It is done with Trackmate, which is an open and extensible platform for single-particle tracking. Spots are localized using the Laplacian of Gaussian (LoG) method, with an estimated spot radius of 2.5 pixels. The intensity threshold is set a bit lower to prevent track fragmentation due to intensity fluctuations. The linear assignment problem (LAP) algorithm is used to form tracks with costs on quality ranging from 0.1 to 0.5. The gap frame is set to 1 to allow temporary disappearance of the molecule, and track merging and splitting are allowed when multiple molecules crossed paths with one another. Binary images are used to locate tracks whose mean positions coincided with values of 1 in the binary image to isolate tracks found only in cells/nuclei.
3. Reading the tracking data: The data obtained from Trackmate analysis shows the number of spots, the frame number of when it is detected and the X-Y-Z coordinates. This data is later used in MATLAB script to determine the length of each track by calculating the number of times each spot is detected and visualizing it using a histogram plot. The quality of spots is measured as a cost function correlated to the size and intensity of spots [48]. The quality of microscopy data is also studied by plotting the intensity of each reported frame.
4. Image segmentation: Nucleus segmentation is achieved in the following way: First, a Gaussian filter is used to reduce the noise present on the image. Next, a primary binary image is generated based on a more lenient threshold. This binary image is then used as a mask over the original image to take out the background. The image with the subtracted background is now intensity thresholded to result in the segmented nuclei. The last part involves a watershed step to separate nuclei that are close together.

5. Tracking: A MATLAB program is created to extract data out of microscopy time-lapses. The script loads the raw data into MATLAB. Once the file is imported, a Z maximum intensity projection is generated. Next, the nuclei in the movie are segmented per frame; this is done to get an idea of where the nuclei are. For each nucleus, a region is extracted and saved to store each nucleus in its separate

movie. For each nucleus and overall the frames, a Gaussian is fit to the image to get a precise localization of the nuclei. The center of mass coordinates of the segmented nuclei is used as initial coordinates for the fit to reduce the fitting time. In the end, the generated coordinates are corrected for stage drift. Stage drift is measured by using the bright field image or fluorescent beads.

6. Drift: Stage drift is obtained from bright-field images using Fiji. Firstly, the noise is reduced using a Gaussian blur. Next, one cell is selected and cut out of the image (preferably a single cell). This cell is then segmented over all the frames by thresholding. Finally, the coordinates for the center of mass of the segmented cells are found using the analyze particles command in Fiji. These coordinates for all the frames can then be saved and used for drift correction.

7. The drift of nucleus: The tracking results generated from MATLAB script are imported to python to perform further analysis. In order to get a more detailed understanding of nuclear movement, the tracks of nuclei were visualized using a 2D random walk. The steps of the nuclear movement were also compared using histograms to study and compare the step size in various experiments.

8. MSD: The MSD was averaged over all the tracks to plot the MSD curve of a particular experiment. The diffusion coefficient and α coefficients were determined from the calculated MSD of the nuclear movement. The relation is given as MSD directly proportional to diffusion coefficient times τ^{α} coefficient.

Chapter 4: CHARACTERIZATION AND STUDY OF DDR DYNAMICS

Experimental Approach and Results

Earlier work in the lab has established techniques to study replisome subunits using single-molecule microscopy techniques [20]. This project aimed at characterizing the effect of DNA damage or DNA stress on the binding kinetics of replisome subunits and the establishment of DDR. To study the effect of DNA damage on the replisome, the replisome subunit Pol δ was studied when cells were treated with UV radiation and compared to untreated cells. Preliminary results, shown in figure 4.1a with untreated YJL11 and 4.1b with UV treated YJL11, suggest that the number of red spots decreases over time, following the initiation of checkpoint signalling, which stops the further replication process until the completion of DNA repair.

It is also expected that RPA bound to ssDNA will increase after UV treatment [5]. The accumulation of this ssDNA is the signalling checkpoint to initiate DNA damage or stress response [5]. The hypothesis is that increasing amounts of ssDNA after UV irradiation will be observable by greater amounts of RPA bound to chromatin. Figures 4.1c and 4.1d shows preliminary results of the untreated ZEY206 and UV-treated ZEY206 strains. The presence of the RPA is consistent in figure 4.1d with the accumulation of ssDNA, indicating DNA stress that has further obstructed the process of replication.

(a)

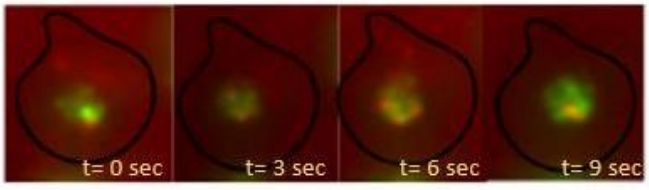

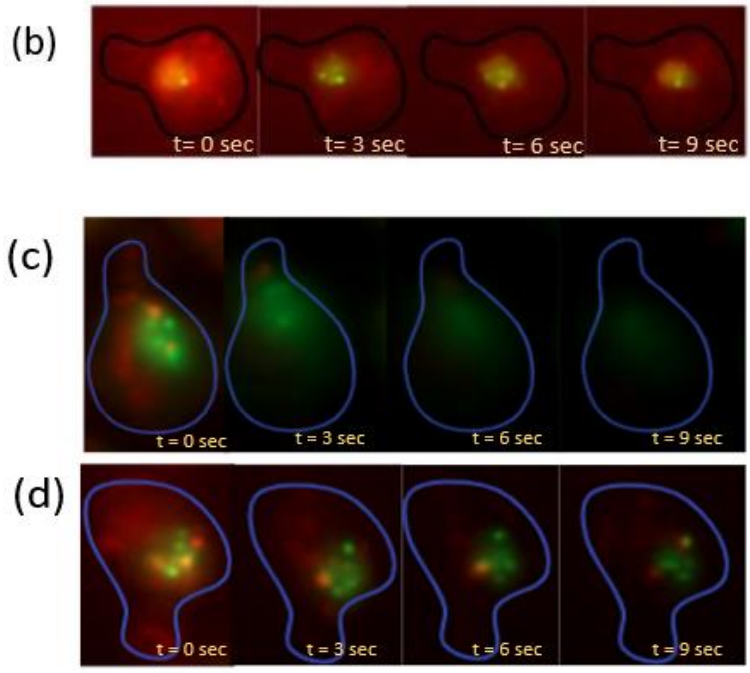

Figure 4.1: The cells entering the S phase shows PCNA mNG in green colour spots, and the protein of interest, Pol δ and RPA, is shown in red colour spots inside the cell (a) Untreated YJL11 with PA-JF549 fluorophore in agarose pad with Optiprep growth medium, (b) YJL11 with PA-JF549 fluorophore in agarose pad with Optiprep growth medium treated with UV light, (c) Untreated ZEY206 with PA-JF549 fluorophore in agarose pad with Optiprep growth medium (d) ZEY206 with PA-JF549 fluorophore in agarose pad with Optiprep growth medium treated with UV light

Once the DDR initiates, multiple kinases associated with the checkpoint response interact with the replisome leading to a signalling cascade [5]. To study the establishment of DDR, multiple strains were constructed carrying C-terminal or N-terminal fusions. Initially, RAD53, DDC2, MRC1 and DUN1 were successfully transformed using BY4743 wildtype. But the tetrads of MEC1 and TEL1, the apical kinases involved in DDR, could not be successfully dissected and gave 2/2 patterns required for selection. Other researchers have favoured the N-terminal fusion for MEC1 and TEL1 [4][6][24][30][38][60]. To test for structural restrictions on the generation of C-terminal

MEC1 and TEL1 fusions, I undertook a bioinformatic analysis of these kinases. Assessing the possible variants of these kinases led to the possibility of growing deleterious strains on transforming them with C-terminal fusion. Additionally, the already constructed strains of RAD53, DDC2, MRC1 and DUN1 were also checked, and as expected, their variants were more tolerable. The variants mentioned here are the single-point mutated genes that were later categorized as tolerant or deleterious based on the calculated SIFT score for the missense mutations and applying statistical methods to determine its probability of mutation or overrepresentation of functional mutation. Table 4.1 shows the number of variants studied against the number of deleterious variants. As described in the literature, the apical kinases have low-confidence or deleterious variants that could lead to the strain losing its functional impact and it generally has a negative effect on the protein structure [22][28][29].

KINASES	NO. OF VARIANTS	COMMENTS
MEC1	14	3 variants are deleterious
RAD53	8	All variants are tolerable
TEL1	14	3 deleterious variants, rest are low confidence tolerated
DDC2	17	All tolerated variants
DUN1	12	All tolerated variants

Table 4.1: Analysis of variants of all the genes involved in DDR

The successfully transformed strains of RAD53, DDC2, MRC1 and DUN1 were confirmed for insertion using the PCR techniques and primers developed for the same. On confirmation, the strains were studied under SMM to look for the proteins in the

desired wavelength. The untreated strains showed highly diffusing single-molecules on being activated by 405 lasers. Figure 4.2 shows the snapshots of these untreated cells after a few seconds of bleaching and being activated by the 405 lasers. Photobleaching is required to diffuse the excess dye from the background and makes it easier to notice the bound fluorescent proteins. The cells have noticeable labelling of the nucleus, which confirms the successful insertion of the genes. Figure 4.2(c) and 4.2(d) for RAD53 and DUN1 show a heterogeneously tagged nucleus as compared to MRC1 and DDC2 in Figures 4.2(a) and 4.2(b). It could be due to various reasons, like the strains required more than 40min incubation time, with the fluorescent dye, in the thermomixer at 30°C and 500 RPM as stated in Chapter 3: Sample preparation for single-molecule microscopy. These strains were finally sequenced to check for any possible mutations. These strains will be used in the future to characterize DDR in live cells. Due to time constrain, the construction of apical kinases, MEC1 and TEL1, is still under process. However, the primers and plasmids required for the procedure are ready for use.

Mec1 is a member of the PIKK family that has the FATC domain at its C terminus. Therefore, many researchers worked on Mec1 alleles that could alter this 30-35 residue FATC domain to determine their function at the C-terminal [30]. For instance, changing the terminal tryptophan to alanine gave rise to sensitivity to temperature and HU in its growth media in vitro. Another example was the cell losing its viability by adding a terminal glycine. Additionally, all these Mec1 variants were less stable than wild-type strains that depicted minimized nuclear localization [22].

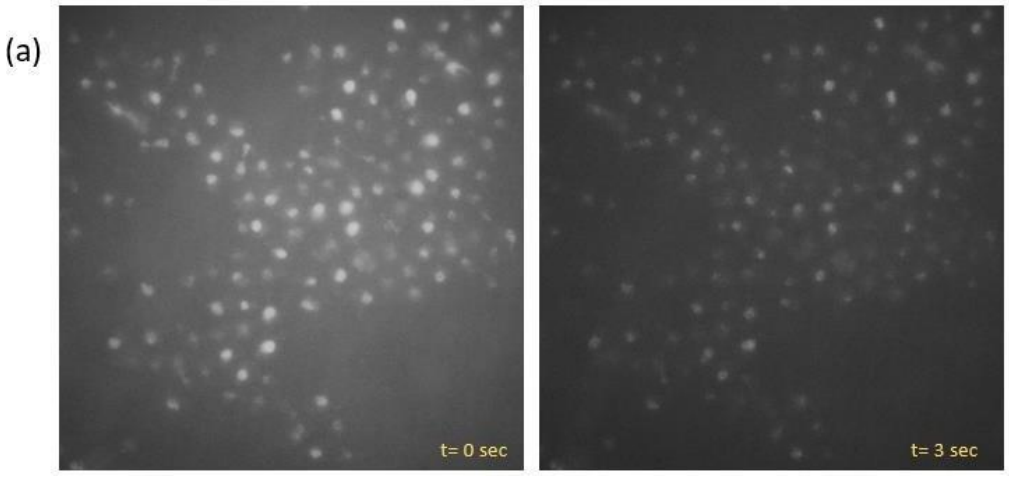

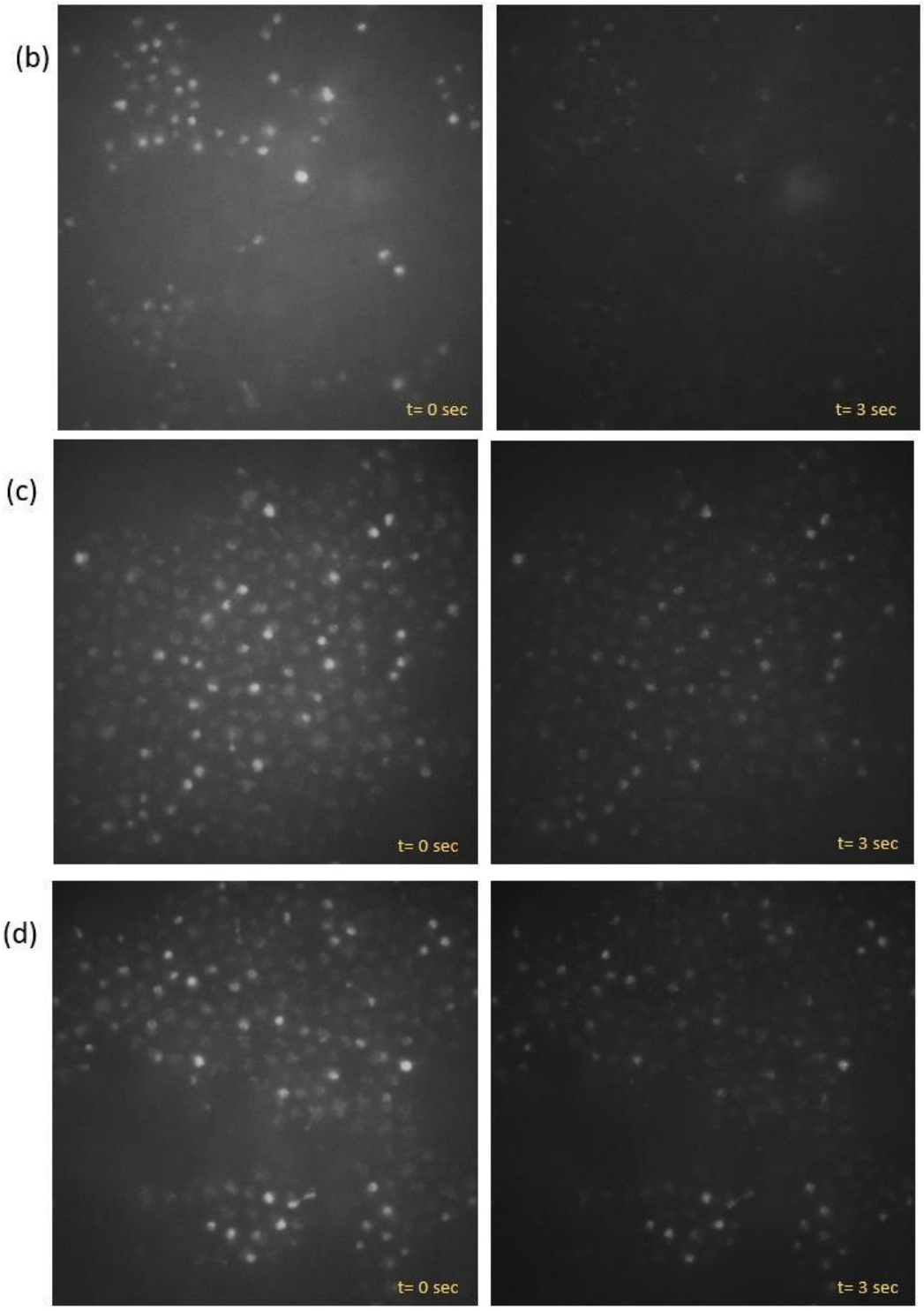

Fig 4.2: The new C terminal strains were constructed and confirmed for insertion by taking snapshots of the fluorescent-tagged nucleus and using JF552 dye. (a) MRC1 without

bleaching and after 3 seconds of bleaching (b) DDC2 without bleaching and after 3 seconds of bleaching (c) RAD53 without bleaching and after 3 seconds of bleaching (d) DUN1 without bleaching and after 3 seconds of bleaching

Alteration of the terminal residues results in stress-related phenotypes and partial mislocalization of the protein to the cytoplasm because the PIKK molecules have hydrophobic terminal residues. Hence researchers worked on the variants altered at C-terminal to verify if the FATC domain has any role in regulating the stability of PIKK family members [30]. They concluded that the mec1 strain is sensitive to temperature and hydroxyurea and shows reduced growth in these conditions. Whereas tagging the wild-type with $Flag^5$ or eGFP tag at the N-terminal did not affect its growth. [22]

As mentioned earlier, the MEC1 and TEL1 strain construction is yet to be completed. The building blocks for this process have been completed and need to be used further to generate N terminal strains. The gRNA and repair or donor oligos for the process have been designed and developed. The HaloTag fragment (at 900bp) and kan resistant fragments (at 1.5kb) are generated using PCR with the concerned primer and pH6HTC, the His HaloTag plasmid, and pKD4, the kan resistant plasmid. The two fragments are ligated with the digested vector plasmid, pUC18, for cloning. gRNA oligos are annealed into these plasmids and transformed into yeast and the plasmids are lastly ejected for a marker-free integration of Halo-tag. The next step in my experiments is to complete the annealing and cloning of the gRNA with the plasmids to construct N-terminal strains.

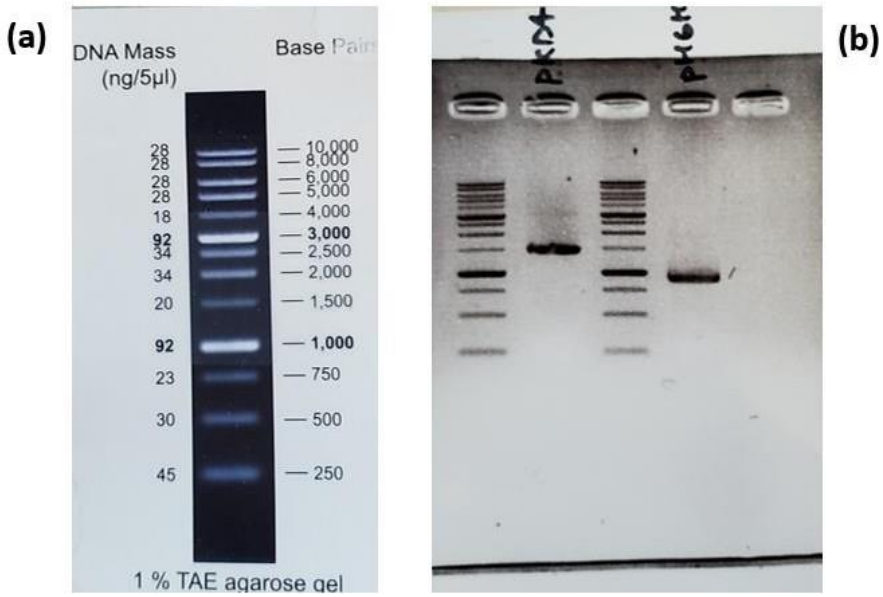

Figure 4.3: PCR to obtain HaloTag fragments at 900bp and kan resistant fragments at 1.5kb required for N terminal fusion (a) Scale to check the fragment and its corresponding number of base pair (b) PCR electrophoresis gel showing the ladder along with pKD4 and pH6HTC

Discussion

The presence of RPA (the visible red spots) in the treated ZEY206 gives a possible indication of the ongoing DDR. Therefore, the quantification of this data could provide important information about the onset of this response. Furthermore, a reduction of Pol δ spots, shown by the red spots in treated YJL11 at the replication fork, would also support the hypothesis that the DDR stops the progress of the replication fork until the damage is repaired.

One of the challenges to study or quantify the DDR using these strains is that after some time, the labelled proteins will start diluting as cells grow and divide, resulting in the loss of the visible red spots. Since part of my focus is to obtain concrete information about the timing after UV treatment for the establishment of DDR. The dilution of labelled protein in this scenario makes the process harder.

The strain construction was one of the most critical and challenging steps in studying the protein dynamics involved in DNA damage response. The strain construction has been a big obstacle that delayed the experiments further. So far, RAD53, DDC2, MRC1 and DUN1 have been successfully transformed, and the MEC1 and TEL1 N-terminal fusion is in process. Additionally, in the entire process of strain construction, the dissections of spores proved to be unsuccessful for a few of the proteins. Multiple repetitions were needed to be sure of the results. These challenges hindered microscopy to a great extent.

As mentioned earlier, the untreated strains with the successfully transformed C terminal proteins had a highly diffusing population of molecules in our experiment using 500ms capture rates, with no clear spots representing chromatin-bound molecules. This supports the literature stating that these proteins bind to the replication fork under stress due to dNTP pool depletion on treating with UV [38]. The strains can be later modified to have PDR5 gene deletion, which has been reported from the previous work in the lab to allow better retention of the dye and makes the imaging with halo ligand much easier [35], which can help tackle the heterogeneity of fluorescent noticed in figure 4.2 above.

Future work for these experiments will include quantifying the data already captured, first to determine the onset of DDR on being treated by UV using Pol δ or RPA. Few other replisome subunits can also be studied to see if they have a similar response to Pol δ. Furthermore, Hydroxyurea or Camptothecin can be used for treating the cells. SMM will also be used to study DDR proteins after treating cells with the above-mentioned reagents. I expect that continuation of this study will generate critical information to help us understand how DDR is established. Simultaneously, the CRISPR Cas9 will be used to successfully transform MEC1 and TEL1 to further study DDR dynamics.

Once all the strains are successfully constructed and tested for insertion, the haploid strains need to be mated with the PCNA mNG. This diploid strain will express PCNA molecules in the green channel with 488nm laser beam, and HaloTag labelled proteins in the red channel with 561nm laser beam on being continuously activated by 405nm laser beam. Later the dynamics of these HaloTag labelled proteins can be studied under the action of UV radiation-induced DNA damage with a similar microscopy protocol.

Chapter 5: FACTORS AFFECTING SMM IN YEAST

Experimental Approach and Results: Choice of Fluorophores

Work in our lab has used fluorescent tags attached to the proteins in question to employ fluorescence microscopy. When attempting to image single molecules, the background fluorescence must be low enough to achieve a high signal-to-noise ratio, which justifies using the HILO microscopy technique [17]. Additionally, the fluorophore used in earlier publications from the lab is the Photoactivable Janelia Farms 549 (PA-JF549) [20] [35]. However, the choice of the fluorophore is one of the significant factors that could affect the quality of data obtained. Hence, using a strain carrying a copy of the histone H3 fused to halo tag (YTK1434), I decided to test various fluorescent dyes available in the lab: PA-JF549, PA-JF646, JF552 and JF646 (Appendix IV).

Trackmate, an inbuilt feature of Fiji and is used to track the single molecules for our experiment [47]. Expediently, Trackmate has an inbuilt feature to identify the intensity spot by fitting the Gaussian model and applying the nearest neighbour approach in terms of cost function [48]. Figure 5.1(a) below shows an example of how the spots are detected at the 24^{th} frame for YTK1434 strain with JF552 dye and agarose with Optiprep as the growth condition. Similarly, upon using Trackmate, the tracks recorded for the same example are shown in figure 5.1(b). Later, the cost function applied for these experiments was “Quality”, which is correlated to the size and intensity of the identified spot. Figure 5.2 shows the quality of spots detected against all the tracks detected in the YTK1434 strain when treated with PAJF549, PAJF646, JF552 and JF646. Similarly, figure 5.3 shows the track length of all the tracks for the same set of experiments.

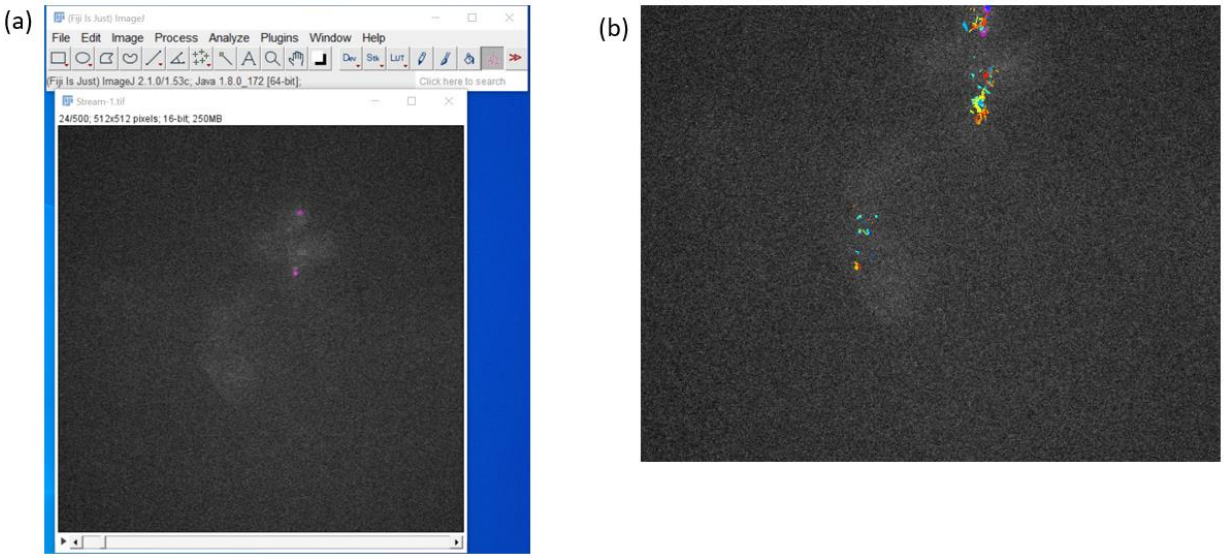

Figure 5.1: Example demonstrating the working of ImageJ-Trackmate: (a) Spot detected at 24th frame for histone H3 with JF552 in Agarose and Optiprep condition, (b) The tracks of all the spots detected over the entire 500 frames for histone H3 with JF552 in Agarose and Optiprep growth condition

The spot quality for the sample with PA-JF549 shows a wider distribution of spot intensity ranging approximately from 0.2X AU 10^6 to 0.75 X AU 10^6 compared to all others. The histogram for the experiment with PA-JF646 shows a peak at 0.5 X AU $10^{6.}$ The experiment with the other non-photoactivable dyes, JF552 and JF646, shows a narrow peak at 0.3 X AU 10^6 with a trailing end. The cells labelled with non-photoactivable dye required a longer pre-bleaching step compared to PA dyes before single molecules were evident. Consequently, the trailing end in the histogram of figures 5.2c and 5.2d may represent spots containing multiple fluorescent molecules.

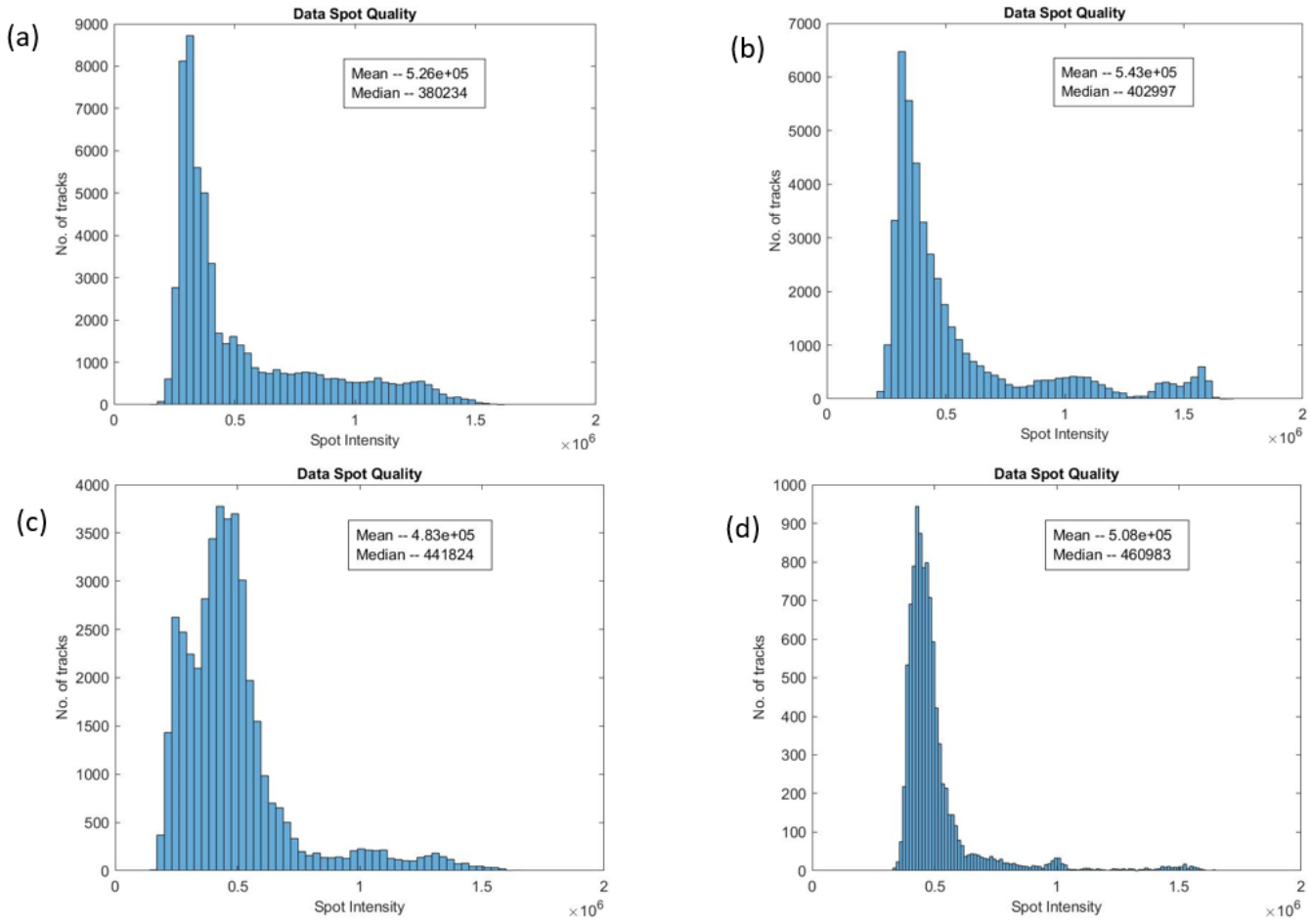

Figure 5.2: Spot quality of the segmented tracks: (a) Histone H3 with JF552, (b) Histone H3 with JF646, (c) Histone H3 with PA-JF549, (d) Histone H3 with PA-JF646

The histogram for the calculated track length shows an exponential decay with a similar time constant as previously determined for PA-JF549 in our lab [2][35]. The majority of tracks in the experiment with PA-JF549 and PA-JF646 are concentrated at the extreme left side of the histogram, meaning most of the tracks have a shorter track length. JF552 has a gentle exponential decay as compared to the photoactivable dyes but is steeper when compared to the experiment with JF646, depicting that the spots are visible for a longer time period.

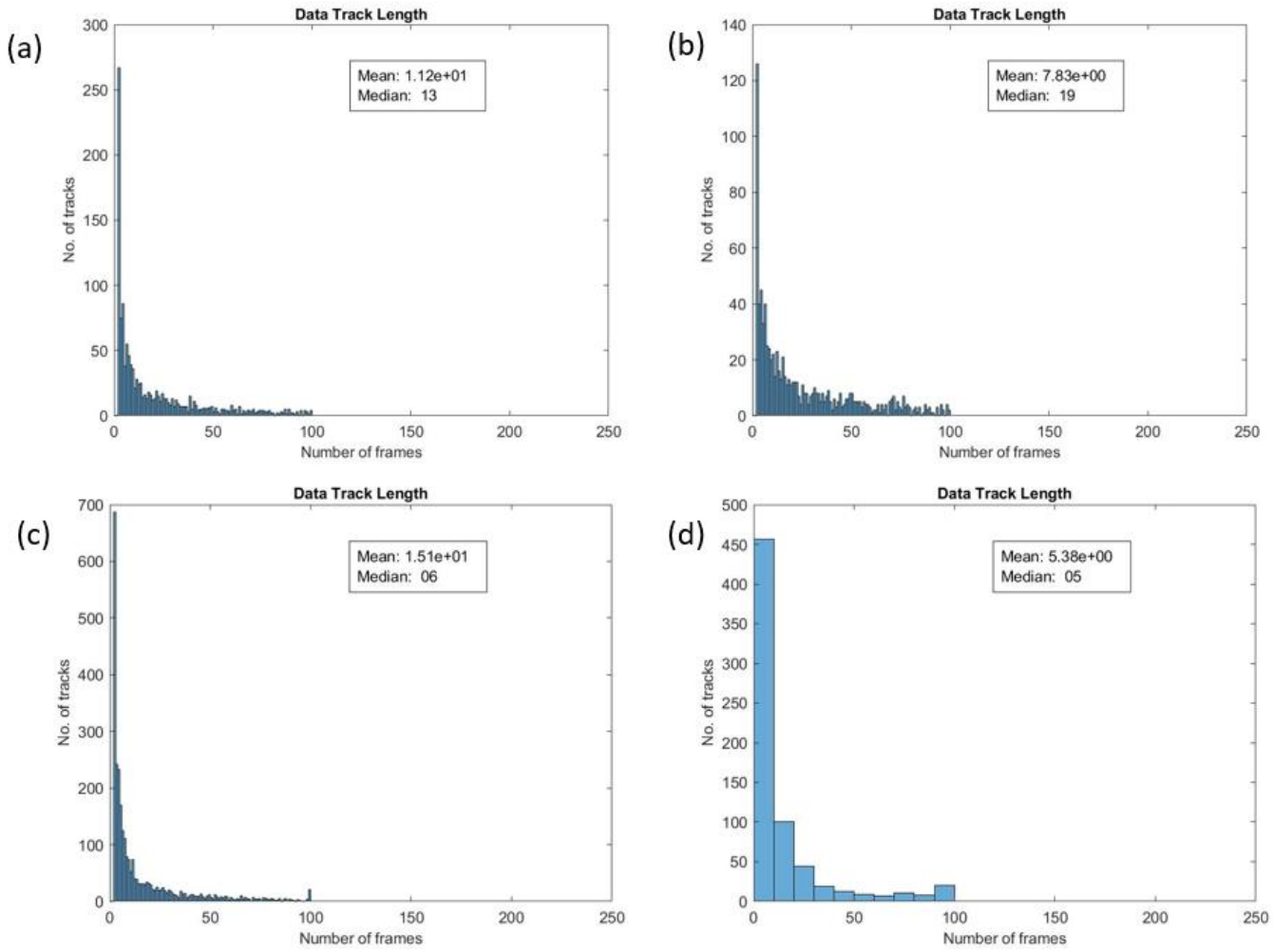

Figure 5.3: Spot track lengths and fluorophore used: (a) Histone H3 with JF552, (b) Histone H3 with JF646, (c) Histone H3 with PA-JF549, (d) Histone H3 with PA-JF646

Table 5.1 shows the quality of data obtained or spots detected in terms of signal-to-noise ratio and mean squared error (MSE). As noticeable from the raw data (figure 5.5), the signal-to-noise ratio was higher for the sample with JF552 dye than all the others. From visual inspection of the images, this may be associated with a lower background fluorescence in the cell. Cellular background fluorescence in PA dyes may result from unspecific binding to cellular structure or from their lower permeability which prevents uncoupled dye from diffusing out of cells [67]. However, the track length of PA-JF549 was

closer to the mean track length of JF552 owing to a similar emission and absorption spectrum. Similarly, the mean track length of PA-JF646 was closer to JF646 and comparatively less than the PA-JF549 and JF552. Thus, according to the data obtained, the PA-JF549 and JF552 dyes perform better than the PA-JF646 and JF646 dyes, regarding background noise interference for tracking the single molecules, since we can track single molecules for a relatively good amount of time.

Fluorophore	**Growth Medium**	**Signal-To-Noise Ratio**	**MSE**	**Mean track length (# frames)**
JF552	Agarose + Optiprep	31.4	1294.9	11.2
JF646	Agarose + Optiprep	30.9	1160	7.83
PA-JF646	Agarose + Optiprep	25.2	1636.5	5.38
PA-JF549	Agarose + Optiprep	25.6	1480.1	15.1
JF549	Agarose + Optiprep	N/A	N/A	N/A

Table 5.1: Analysis of the quality of raw data of histone H3 with all the fluorescent dyes

I was unable to detect any single-molecule spots in similar experiments using the non-photoactivable dye JF549 dye. This is possibly due to the low cell permeability of this dye, although I cannot discard other explanations. This dye was removed from further studies.

Experimental Approach and Results: Autofluorescence, Cell Wall and Choice of Growth Conditions

Yeast exhibits higher autofluorescence background compared to *E. coli*, as seen in figure 5.4. Although multiple factors, such as the difference in their metabolism, contribute to the heightened background, here I focused on the contribution from its thicker cell wall (~200nm) compare to the ~10nm thick cell wall of bacteria [20]. A thick cell wall can contribute to the refraction of the fluorescence light produced in cells, resulting in a lower light collection. Optiprep has previously been used to match the refractive index of biological samples to improve microscopy [68]. Adding Optiprep to a concentration of 30% results in a refractive index similar to that of the cell wall of yeast [35].

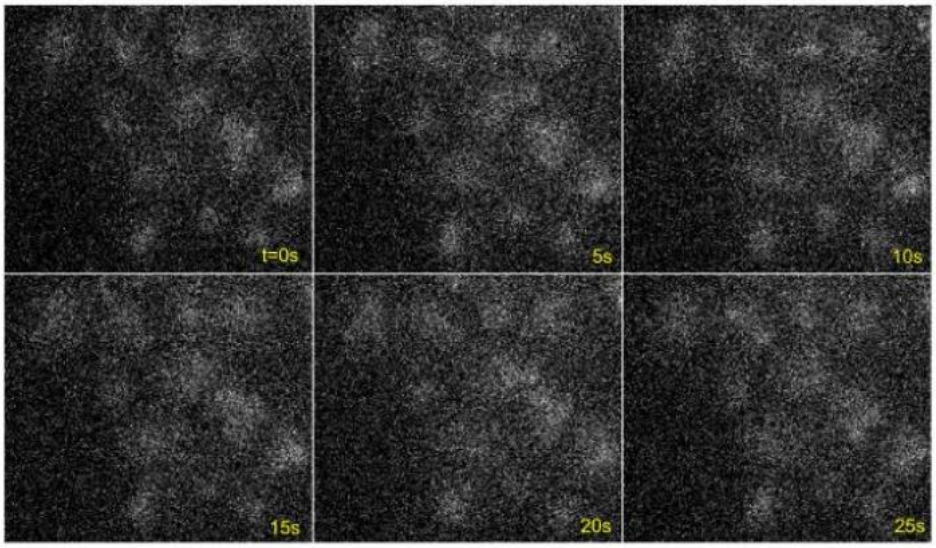

Figure 5.4: Background autofluorescence in histone H3

The data collected from the experiments for various fluorophores and varying growth conditions were studied for the spot quality and track length, as we can see from Appendix VI. For all the four dyes, the spot quality of the sample without using Optiprep showed a smaller second peak. In addition, the trailing end of the histogram from the experiment with agarose was not detected while using ConA for slide preparation. Thus, the experiment with ConA provides a precise, narrow distribution of spot intensity or

quality. Additionally, the track length of all these experiments also shows an exponential decay in a similar trend.

When the data were evaluated and compared for all the experiments, it was noticed that the ConA gave a higher signal-to-noise ratio with a lower MSE as compared to the experiments with agarose. As we can observe from table 5.2, data from experiments with agarose and Optiprep showed a similar signal-to-noise ratio to that of ConA but presented considerably higher MSE for experiments when agarose and Optiprep were used. The mean track length of the single molecules segmented is higher for the agarose with SC growth condition than the one with Optiprep and ConA for all the dyes. However, for the PA-JF646 and JF646, the mean track length is considerably lower for ConA and agarose with Optiprep condition and rises considerably when using SC with Agarose. But the PA-JF549 and JF552 dyes have a comparatively similar range of mean track length for all three different conditions.

Growth Medium		**Fluorophore**	**Signal To Noise Ratio**	**MSE in terms of intensity**	**Mean track length (# frames)**
Agarose	Optiprep	JF552	31.4	1294.9	11.2
Agarose	SC	JF552	22.58	1968.78	16.7
ConA	SC	JF552	37.42	312.01	9.88
Agarose	Optiprep	JF646	30.9	1160	7.83
Agarose	SC	JF646	22.02	3220.037	27.6
ConA	SC	JF646	31.93	636.5	13.5

Agarose	Optiprep	PA- JF646	25.2	1480.1	5.38
Agarose	SC	PA- JF646	24.99897	2604.539	21.5
ConA	SC	PA- JF646	26.82	501.22	6.18
Agarose	Optiprep	PA-JF549	25.6	1636.5	15.1
Agarose	SC	PA-JF549	23.66	2419.1	18.7
ConA	SC	PA-JF549	33.08	512.27	10.4
Agarose	Optiprep	JF549	N/A	N/A	N/A
Agarose	SC	JF549	N/A	N/A	N/A

Table 5.2: Analysis of the quality of raw data of histone H3 with all the fluorescent dyes and different growth conditions

Figure 5.5 below shows an example of the raw data acquired for three different growth conditions, namely with ConA with SC, Agarose with Optipre and Agarose with SC and for four different fluorophores, i.e., JF552, JF646, PA-JF549 and PA-JF646, at a random given time t=52 sec.

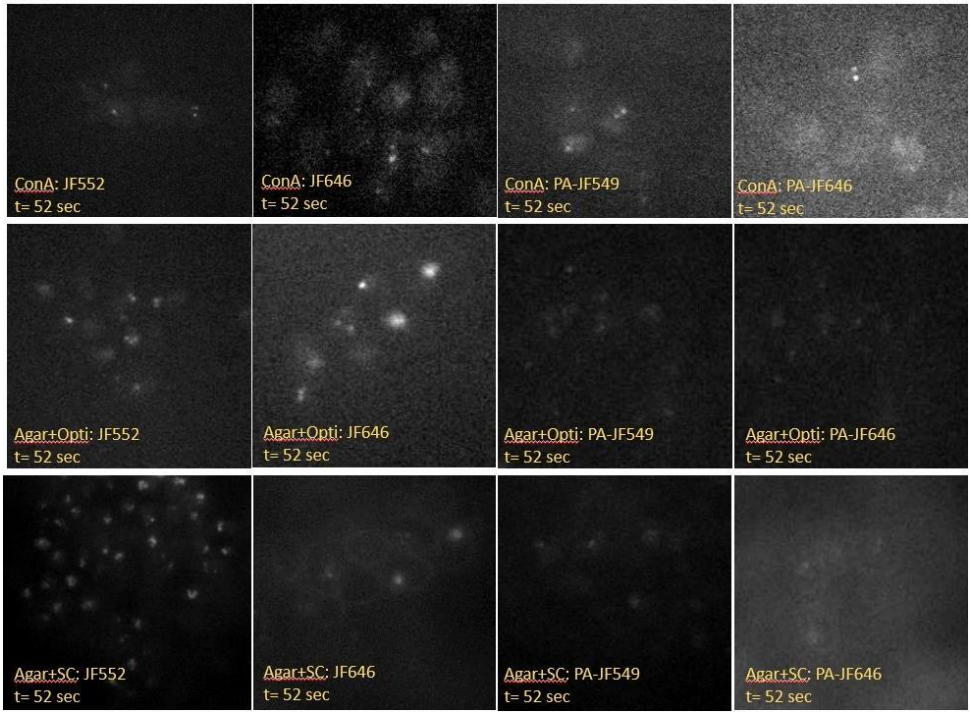

Figure 5.5: Example of images from experiments with three growth conditions, (top to down) ConA+SC, Agarose+Optiprep and Agarose+SC, and four different dyes, (left to right) JF552, JF646, PA-JF549 and PA-JF646

Discussion

The data used in these experiments contain spots that are certainly not single, along with other spots that may be from the background or from a cell that does not exhibit the single-molecule nature after bleaching. These spots can result in the trailing end that we notice in our figures. For future work, these spots can be cleaned for, and the scrutinized data can be analyzed only for the spots that are positively from single molecules.

The non-photoactivable dyes require longer pre-bleaching steps during the experiments to reduce the density of fluorescent molecules. Detection of single molecules was facilitated by a lower background than that when photoactivable dyes were used,

during 405nm laser activation. As a result, JF552 is the best performing fluorescent dye among all five dyes used in these experiments.

Similarly, using Optiprep with agarose pad was able to tackle autofluorescence compared to experiment with agarose pad without Optiprep. Optiprep removes a shadow produced by the thick cell wall of yeast, but agarose too added to background noise. Although not very high, this background noise was not noticed when the ConA was used for slide preparation. Consequently, these results prompt us to stop using agarose to immobilize cells in single-molecule microscopy.

The long track length when using Agarose and SC for PA-JF646 and JF646 needs to be verified with more experiments and quantification to reach a definite conclusion.

Future studies may combine ConA with Optiprep to test for a potential further improvement in the quality of data acquired. This characterization will also be extended by testing other imaging protocols (for example, using 10 ms capture rates) and by characterizing photoactivatable fluorescent proteins such as mMaple and mEos3.2.

Chapter 6: EFFECTS OF NUCLEAR MOVEMENT IN YEAST AND OTHER BIOLOGICAL FACTOR AFFECTING THE MOVEMENT

Experimental Approach and Results

Stage drift usually accounts for the small percentage of drift in the raw data of yeast microscopy. But the movement of the nucleus can also cause drift and lead to the movement of spots out of the focal plane. Since the replisome subunits are present in the somewhat centrally placed nucleus, any movement can result in drifting the data. In addition, the nucleus is surrounded by various other cell organelles, like mitochondria, ER, cytoskeletal structure, etc. These can either restrict or assist the movement of the nucleus. The literature describes that actin and microtubule affect the movement of the nucleus in fission yeast, and this movement differs in various stages of the cell cycle [37].

To measure nuclear movement in budding yeast, we used a strain carrying a fluorescent derivative of the histone H2B (H2B-GFP fusion). A similar strain was used to study the nuclear movement in fission yeast. We then took pictures of cells with 1-second intervals and tracked the movement of the nucleus by determining the centroid of the fluorescent shape generated (Figure 6.1). From this, I generated tracks representing the movement of the nucleus over time and calculated the diffusion coefficient and the α coefficient (Figure 6.2 and Table 6.1). As can be observed in my results, the nucleus of fission yeast showed more constrained movement as compared to the budding yeast, as reported from lower values of the diffusion coefficient and α coefficient (Table 6.1). I also noticed that both of these parameters were higher in the S/G2 phase compared to the G1 phase in budding yeast. This comparison can be noticed in Appendix V.

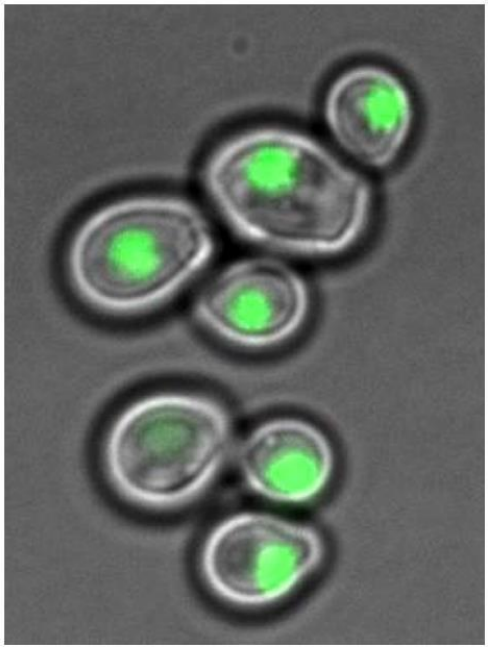

Figure 6.1: Depicting the budding yeast cell showing the mNeonGreen fluorescent nucleus of budding yeast

To test for potential participation of the cytoskeleton in the control of nuclear movement, similarly to fission yeast, budding yeast was treated with nocodazole to inhibit microtubule and with latrunculin A to inhibit actin. The 2D random walk graph in figure 6.2 clearly shows the movement of nocodazole-treated cells against the untreated and latrunculin A-treated cells. On average, the tracks for the treated cells explore less space than the tracks in untreated cells for the same amount of time. However, the latrunculin A-treated cells are far more constrained than the nocodazole-treated cells. Similarly, the movement of cells in the G1 phase for all three experiments is less than the S/G2 phase, irrespective of the treatment.

Multiple histograms shown in Appendix V show the average and maximum step size of the nuclear movement. The histogram for the untreated cells in the G1 phase has a smaller average of step size. The nocodazole-treated cells in both stages show similar characteristics as that of untreated cells in the S/G2 phase. A similar trend is noticed in

the case of cluster graphs and MSD plots. In the case of latrunculin A-treated cells, the average is smaller for both phases.

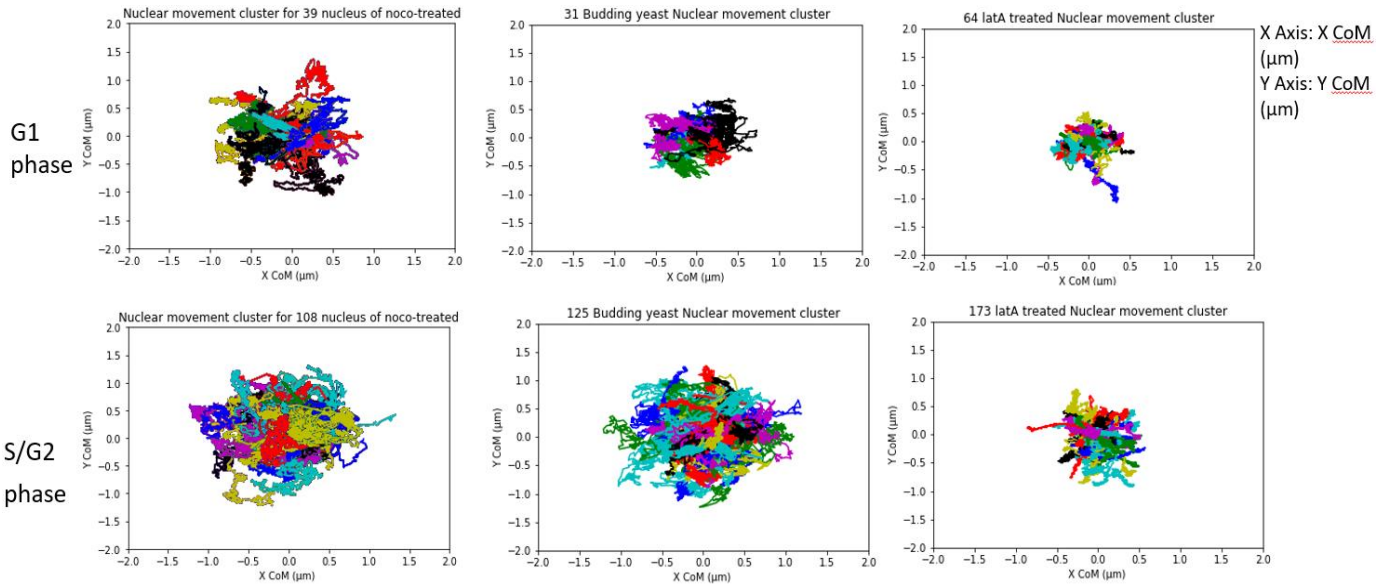

Figure 6.2: 2D random walk graph untreated and treated budding yeast. The first row shows all the cells in the G1 phase for all three experiments. The second row shows all the cells in the S/G2 phase for all three experiments. The first column shows the experiment of budding yeast treated with Nocodazole; the second column is the experiment with untreated budding yeast, the third column is the experiment with budding yeast treated with latrunculinA

The diffusion coefficient and MSD yield information about the movement and characteristics of the different molecules. Moreover, diffusion has a linear relation with time. The mean square displacement can be physically interpreted to measure how much space the particle has explored in a specific window of time. When fitting the MSD to the function describing the diffusion coefficient, a value of 0.6209 and 0.7727 for G1 and S/G2 phases was found for α, as shown in figure 6.3, which is expectedly in the range for subdiffusive motion. Subdiffusive behaviour by the nucleus agrees with what has been reported for other particles in the cell [41].

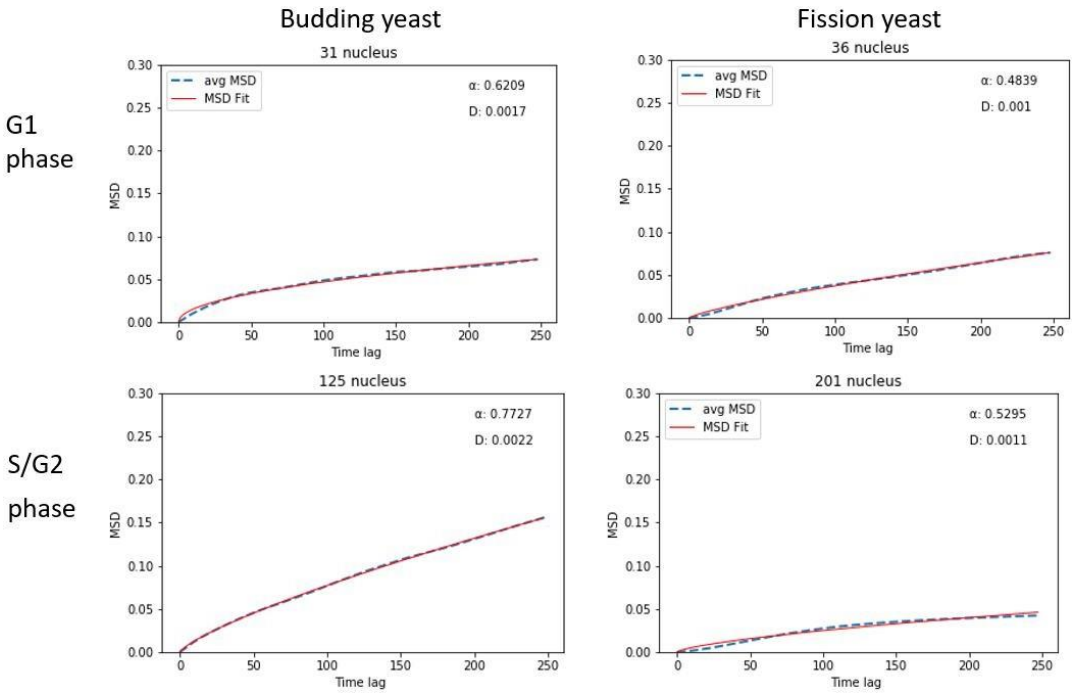

Figure 6.3: Shows the average MSD of all the tracks, and the red line indicates the fitting of the curve to determine its diffusion coefficient and α coefficient

Similarly, as shown in Table 6.1, the α coefficient for the G1 phase for all the experiments is lower than that of cells from the S/G2 phase, although the magnitude of the difference is smaller than in untreated cells. These results suggest fewer restrictions in the movement of the nucleus in the latter phases of the cell cycle, although it may also account for an increased cell volume as cells progress through the cell cycle. Additionally, on treating the cell with nocodazole and inhibiting the microtubule, the α coefficient of the movement remains similar to that of untreated cells. Whereas the α coefficient of latrunculin-treated cells decreases considerably, supporting the constrained 2D random walk graph.

	Phase	Sample size	α coefficient	Diffusion coefficient ($\mu m^2/sec$)
Budding Yeast	G1	31	0.6209	0.0017
	S/G2	125	0.7727	0.0022
Fission Yeast	G1	36	0.4839	0.001
	S/G2	201	0.5295	0.0011
Nocodazole treated budding yeast	G1	39	0.7678	0.0019
	S/G2	108	0.7778	0.002
Latrinculin-A treated budding yeast	G1	64	0.2072	0.0002
	S/G2	173	0.2543	0.0001

Table 6.1: Analysis of sub-diffusive movement of the nucleus budding yeast cells in all the experiments for two different stages of cell cycle

H2B-GFP cells were fixed and imaged to test the precision of the generated localization scripts. The time-lapses with fixed cells were analyzed through the program to see if there are deviations in localizations. A perfect program would locate the fixed nucleus at the same x- and y-coordinate, but there are always some tiny deviations in reality. Figures in Figure 6.4 show a comparison between a moving nucleus and a fixed nucleus. It can be seen that the distance the nucleus moves per frame is more significant

for the live cell than the end-to-end distance of the fixed track. This analysis confirmed that deviations in localizations caused by the program would not substantially impact the generated data. Additionally, the results from the fixed yeast samples were used to correct the experimental drift in the measurements for the movement of the live yeast samples.

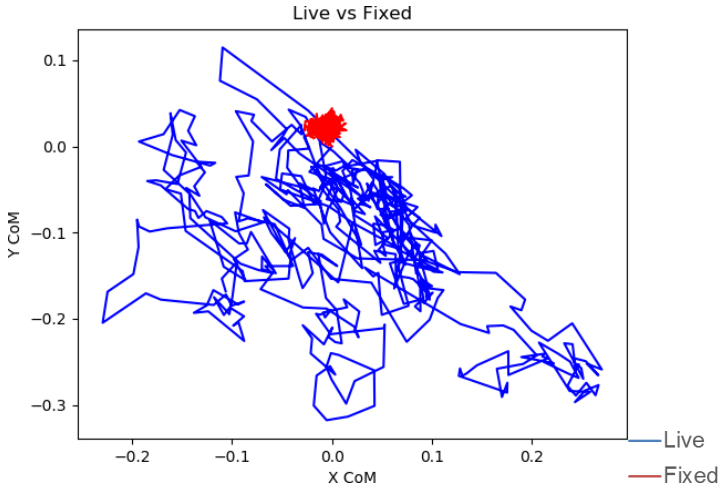

Figure 6.4: An example of live vs fixed budding yeast nucleus. The spread-out blue random walk graph shows the movement of a nucleus of live budding yeast, and the constraint red random walk graph shows the movement of the nucleus of fixed budding yeast.

Discussion

The results indicate that the nucleus of *S. cerevisiae* is quite mobile. It was shown the nucleus has sub-diffusive behaviour and can be modelled as a fractional Brownian motion process. Although these results are generated from 2D images, it can be assumed that the motion applies in 3D, but this still needs to be verified to be sure. It was found that the nucleus moves approximately 400nm in 200sec. 400nm is the focal depth of the microscope, so after 200 seconds, the nucleus has, on average, moved out of focus. This data is crucial in experiments where bound times are to be determined, and if the bound times are close to or over 200 seconds, the resulting data can have a few uncertainties.

So for proteins that bind for a long time, for instance, the helicase, it is essential to sample at multiple focal planes at the cost of increased bleaching.

The nuclear movement in all the experiments depicts a subdiffusive regime, i.e. below α coefficient of 1, owing to its environment. The nucleus in budding yeast moves more freely than in the fission yeast that shows a constrained directional movement. We presume that the directional movement is due to the rod shape of fission yeast. My analysis of the nucleus in fixed cells showed some error movement, and it was used as a reference for the localized precision of the live cells. Furthermore, the untreated cells show a noticeable difference in nuclear movement in different phases. One possible interpretation of these results is possible changes in the cell environment over the cell cycle, resulting in changes in nuclear diffusion. However, future work will explore a possible contribution from the cell size in these estimates.

The treatment with latrunculinA has a significant effect on the nuclear movement, suggesting that actin plays a substantial role in the nuclear movement in budding yeast. While on the contrary, upon treating with nocodazole to inhibit microtubules, there is no significant change in the movement, other than the fact that cells in G1 and G2/S phases reported more similar parameters among them, behaving similarly to untreated cells in the S/G2 phase. Thus, the nuclear movement doesn't show much difference in different cell cycle stages for nocodazole or latrunculin-treated cells. Although understanding the mechanisms behind the dynamics of the nucleus of *S. cerevisiae* goes beyond the scope of my thesis, this is an exciting subject represented only scarcely by the literature.

Chapter 7: CONCLUSION

This thesis made advances towards characterizing and understanding the dynamics of DNA damage response in the eukaryotic replisome of *S. cerevisiae*. Despite many technical difficulties encountered in chapter 4, suitable strains with the desired gene and halo tag insertion were constructed and were imaged using suitable conditions for the single-molecule microscopy techniques. It appears that this technique is best suited for the study of proteins that exhibit an organized structure and concentrated distribution, which ensure adequate signal intensity for reliable image reconstruction. Chapter 4 implemented SMM to determine the binding kinetics of Pol δ, RPA, and a few checkpoint mediated kinases in times of DNA damage or stress. This preliminary work suggests the treatment of cells with UV leads to the inhibition of the DNA polymerases, resulting in the accumulation of ssDNA. RPA binding to the accumulated ssDNA signals the checkpoint kinases about the encountered stress. Hence, these RPA can be used to study or quantify the onset of DDR. This work also supports the hypothesis that DDR will obstruct the process of the replication fork until the damage is repaired. Preliminary characterization of the new strains in Chapter 4 also suggests that the DDR proteins are highly diffusive and will not bind to the fork unless a DDR is initiated. Future studies, using the improved methods described in Chapter 5, will aim at obtaining a clearer description of the replisome after DNA damage and of the behaviour of DDR proteins during the establishment of DDR.

Chapter 5 analyzed the effect of various factors like the type of fluorophore, the presence of cell wall in yeast, and auto-fluorescence in single-molecule microscopy of yeast. Our results are in agreement with previous observations that the presence of a thick cell wall of yeast affecting the quality of acquired data. This challenge is overcome by using Optiprep in the growth medium. However, an alternative technique by employing ConA for slide preparation to avoid using agarose gel proved to be an even more effective solution. Chapter 5 also discusses the quality of data with five different fluorescent dyes.

These experiments conclude that JF552 is currently the best available dye for single-molecule data.

Chapter 6 discusses the effect of nuclear movement in order to avoid drift in the data. It also discusses the effect of the cytoskeleton on the nuclear movement within the cell. The cytoplasm of the cell is a viscoelastic medium, and given the size scale of the nucleus, this results in its constrained movement. The cytoplasm also consists of multiple organelles and polymer networks which all probably interfere with the movement of the nucleus. The experiment shows that the cell exhibits prominent nuclear movement, and inhibiting the microtubule by treating it with nocodazole does not really have any significant effect on this movement. But that actin may play a role in controlling nuclear movement.

The research of this thesis holds broader implications for the understanding of DNA damage response in yeast and for the improvement of the single-molecule microscopy technique for yeast. Characterization of the binding kinetics of DDR factors is normally growing, and in cells experiencing DNA damage will allow us to better understand how the cell integrates the information on the state of its genome, eventually leading to a decision of establishing DDR. By integrating the results of aim3 with aim1 or aim2, could lead to clear data and better analysis. Indeed, the optimization of single-molecule imaging for the yeast system provides a more efficient and powerful approach to not only study the eukaryotic replication and DDR but also other processes occurring in the nucleus.

REFERENCES

[1] Johnson A., O'Donnel M. Cellular DNA replicases: components and dynamics at the replication fork. DOI: 10.1146/annurev.biochem.73.011303.073859

[2] Nitin Kapadia, Ziad W. El-Hajj, Rodrigo Reyes-Lamothe. Bound2Learn: A Machine Learning Approach for Classification of DNA-Bound Proteins from Single-Molecule Tracking Experiments. doi: https://doi.org/10.1101/2020.02.20.958512

[3] Di Lazzaro V, Profice P, Pilato F, Capone F, Ranieri F, Pasqualetti P, Colosimo C, Pravatà E, Cianfoni A, Dileone M. Motor cortex plasticity predicts recovery in acute stroke. DOI: 10.1093/cercor/bhp216

[4] Enrico Baroni, Valeria Viscardi, Hugo Cartagena-Lirola, Giovanna Lucchini, and Maria Pia Longhese. The function of budding yeast Sae2 in the DNA damage response requires Mec1 and Tel1 dependent phosphorylation. Mol Cell Biol. 2004 May; 24(10): 4151–4165.; doi: 10.1128/MCB.24.10.4151-4165.2004

[5] Rachel Jossen and Rodrigo Bermejo. The DNA damage checkpoint response to replication stress: A game of forks. Front Genet. 2013; 4: 26; doi: 10.3389/fgene.2013.00026

[6] Jennifer A. Cobb, Lotte Bjergbaek, Kenji Shimada, Christian Frei, and Susan M. Gasser. DNA polymerase stabilization at stalled replication forks requires Mec1 and RecQ helicase Sgs1. EMBO J. 2003 Aug 15; 22(16): 4325–4336.; doi: 10.1093/emboj/cdg391

[7] C. Lucca, F. Vanoli, C. Ramusino, A. Pellicioli, G. Liberi, J. Haber, M. Foiani. Checkpoint-mediated control of replisome-fork association and signalling in response to replication pausing. Oncogene, 23 (2004), pp. 1206-1213

[8] Matthew L Bochman and Anthony Schwacha. The mcm2-7 complex has in vitro helicase activity. Molecular cell, 31(2):287-293, 2008.

[9] Jingchuan Sun, Yi Shi, Roxana E Georgescu, Zuanning Yuan, Brian T Chait, Huilin Li, and Michael E O'donnell. The architecture of a eukaryotic replisome. Nature structural & molecular biology, 22(12):976-982, 2015.

[10] Ivar Ilves, Tatjana Petojevic, James J Pesavento, and Michael R Botchan. Activation of the mcm2-7 helicase by association with cdc45 and gins proteins. Molecular cell, 37(2):247-258, 2010.

[11] Joseph TP Yeeles, Tom D Deegan, Agnieszka Janska, Anne Early, and John FX Diffey. Regulated eukaryotic DNA replication origin ring with puried proteins. Nature, 519(7544):431-435, 2015.

[12] Thomas A Kunkel and Peter M Burgers. Delivering nonidentical twins. Nature structural & molecular biology, 21(8):649-651, 2014.

[13] Olga Chilkova, Peter Stenlund, Isabelle Isoz, Carrie M Stith, Pawel Grabowski, Else-Britt Lundstrom, Peter M Burgers, and Erik Johansson. The eukaryotic leading and lagging strand DNA polymerases are loaded onto primer-ends via separate mechanisms but have comparable processivity in the presence of pcna. Nucleic acids research, 35(19):6588{6597, 2007.

[14] Nina Y Yao and Mike O'Donnell. The rfc clamp loader: structure and function. In The Eukaryotic Replisome: a Guide to Protein Structure and Function, pages 259-279. Springer, 2012.

[15] Luca Pellegrini. The pol α-primase complex. In The eukaryotic replisome: a guide to protein structure and function, pages 157-169. Springer, 2012.

[16] Agnieszka Gambus, Frederick Van Deursen, Dimitrios Polychronopoulos, Magdalena, Foltman, Richard C Jones, Ricky D Edmondson, Arturo Calzada, and Karim Labib. A key role for ctf4 in coupling the mcm2-7 helicase to dna polymerase within the eukaryotic replisome. The EMBO journal, 28(19):2992-3004, 2009.

[17] Makio Tokunaga, Naoko Imamoto, and Kumiko Sakata-Sogawa. Highly inclined thin illumination enables clear single-molecule imaging in cells. Nature methods, 5(2):159-161, 2008.

[18] Takashi Funatsu, Yoshie Harada, Makio Tokunaga, Kiwamu Saito, and Toshio Yanagida. Imaging of single fliuorescent molecules and individual atp turnovers by single myosin molecules in aqueous solution. Nature, 374(6522):555, 1995.

[19] Makio Tokunaga, Kazuo Kitamura, Kiwamu Saito, Atsuko Hikikoshi Iwane, and Toshio Yanagida. Single molecule imaging of fluorophores and enzymatic reactions achieved by objective-type total internal reflection fluorescence microscopy. Biochemical and biophysical research communications, 235(1):47-53, 1997.

[20] Thomas R Beattie, Nitin Kapadia, Emilien Nicolas, Stephan Uphoff , Adam JM Wollman, Mark C Leake, and Rodrigo Reyes-Lamothe. Frequent exchange of the dna polymerase during bacterial chromosome replication. Elife, 6:e21763, 2017.

[21] Georgyi V Los, Lance P Encell, Mark G McDougall, Danette D Hartzell, Natasha Karassina, Chad Zimprich, Monika G Wood, Randy Learish, Rachel Friedman Ohana, Marjeta Urh, et al. Halotag: a novel protein labeling technology for cell imaging and protein analysis. ACS chemical biology, 3(6):373-382, 2008.

[22] Laughery MF, Hunter T, Brown A, Hoopes J, Ostbye T, Shumaker T, Wyrick JJ. New vectors for simple and streamlined CRISPR-Cas9 genome editing in Saccharomyces cerevisiae. Yeast. 2015 Dec;32(12):711-20. doi: 10.1002/yea.3098. Epub 2015 Sep 21. PMID: 26305040; PMCID: PMC4715497.

[23] Adames NR, Gallegos JE, Peccoud J. Yeast genetic interaction screens in the age of CRISPR/Cas. Curr Genet. 2019 Apr;65(2):307-327. doi: 10.1007/s00294-018-0887-8. Epub 2018 Sep 25. PMID: 30255296; PMCID: PMC6420903.

[24] Roggenkamp E, Giersch RM, Wedeman E, Eaton M, Turnquist E, Schrock MN, Alkotami L, Jirakittisonthon T, Schluter-Pascua SE, Bayne GH, Wasko C, Halloran M, Finnigan GC. CRISPR-UnLOCK: Multipurpose Cas9-Based Strategies for Conversion of Yeast Libraries and Strains. Front Microbiol. 2017 Sep 20;8:1773. doi: 10.3389/fmicb.2017.01773. PMID: 28979241; PMCID: PMC5611381.

[25] Callegari AJ, Kelly TJ. UV irradiation induces a postreplication DNA damage checkpoint. Proc Natl Acad Sci U S A. 2006 Oct 24;103(43):15877-82. doi: 10.1073/pnas.0607343103. Epub 2006 Oct 16. PMID: 17043220; PMCID: PMC1613229.

[26] Liew LP, Lim ZY, Cohen M, Kong Z, Marjavaara L, Chabes A, Bell SD. Hydroxyurea-Mediated Cytotoxicity Without Inhibition of Ribonucleotide Reductase. Cell Rep. 2016 Nov 1;17(6):1657-1670. doi: 10.1016/j.celrep.2016.10.024. PMID: 27806303; PMCID: PMC5134839.

[27] Savas S, Kim DY, Ahmad MF, Shariff M, Ozcelik H. Identifying functional genetic variants in DNA repair pathway using protein conservation analysis. Cancer Epidemiol Biomarkers Prev. 2004 May;13(5):801-7. PMID: 15159313.

[28] Gonzalez-Perez A, Mustonen V, Reva B, Ritchie GR, Creixell P, Karchin R, Vazquez M, Fink JL, Kassahn KS, Pearson JV, Bader GD, Boutros PC, Muthuswamy L, Ouellette BF, Reimand J, Linding R, Shibata T, Valencia A, Butler A, Dronov S, Flicek P, Shannon NB, Carter H, Ding L, Sander C, Stuart JM, Stein LD, Lopez-Bigas N; International Cancer Genome Consortium Mutation Pathways and Consequences Subgroup of the Bioinformatics Analyses Working Group. Computational approaches to identify functional genetic variants in cancer genomes. Nat Methods. 2013 Aug;10(8):723-9. doi: 10.1038/nmeth.2562. PMID: 23900255; PMCID: PMC3919555.

[29] Putnam CD, Allen-Soltero SR, Martinez SL, Chan JE, Hayes TK, Kolodner RD. Bioinformatic identification of genes suppressing genome instability. Proc Natl Acad Sci U S A. 2012 Nov 20;109(47):E3251-9. doi: 10.1073/pnas.1216733109. Epub 2012 Nov 5. PMID: 23129647; PMCID: PMC3511103.

[30] DaSilva LF, Pillon S, Genereaux J, et al. The C-terminal residues of Saccharomyces cerevisiae Mec1 are required for its localization, stability, and function. *G3 (Bethesda)*. 2013;3(10):1661-1674. Published 2013 Oct 3. doi:10.1534/g3.113.006841

[31] Dulin, D., Lipfert, J., Charl Moolman, M. & Dekker, N.H. (2013). Studying genomic processes at the single-molecule level: introducing the tools and applications. Nat. Rev. Gen. 14: 9-22.

[32] Patterson, G., Davidson, M., Manley, S. & Lippincott-Schwartz, J. (2010). Superresolution imaging using single-molecule localization. *Annu. Rev. Phys. Chem*. **61**: 345-367.

[33] Rines, D.R., Thomann, D., Dorn, J.F., Goodwin, P. & Sorger, P.K. (2011). Live cell imaging of yeast. Cold Spring Harb. Protoc. 9: 1026-1041.

[34] Nitin Kapadia, Rodrigo Reyes-Lamothe; A quest for coordination among activities at the replisome. *Biochem Soc Trans* 30 August 2019; 47 (4): 1067–1075. doi: https://doi.org/10.1042/BST20180402

[35] Kapadia N, El-Hajj ZW, Zheng H, Beattie TR, Yu A, Reyes-Lamothe R. Processive Activity of Replicative DNA Polymerases in the Replisome of Live Eukaryotic Cells. Mol Cell. 2020 Oct 1;80(1):114-126.e8. doi: 10.1016/j.molcel.2020.08.014. Epub 2020 Sep 10. PMID: 32916094.

[36] Brouwer I, Patel HP, Meeussen JVW, Pomp W, Lenstra TL. Single-Molecule Fluorescence Imaging in Living *Saccharomyces cerevisiae* Cells. *STAR Protoc*. 2020;1(3):100142. Published 2020 Oct 17. doi:10.1016/j.xpro.2020.100142

[37] Ding DQ, Chikashige Y, Haraguchi T, Hiraoka Y. Oscillatory nuclear movement in fission yeast meiotic prophase is driven by astral microtubules, as revealed by continuous observation of chromosomes and microtubules in living cells. J Cell Sci. 1998 Mar;111 (Pt 6):701-12. PMID: 9471999.

[38] Forey R, Poveda A, Sharma S, Barthe A, Padioleau I, Renard C, Lambert R, Skrzypczak M, Ginalski K, Lengronne A, Chabes A, Pardo B, Pasero P. Mec1 Is Activated at the Onset of Normal S Phase by Low-dNTP Pools Impeding DNA Replication. Mol Cell. 2020 May 7;78(3):396-410.e4. doi: 10.1016/j.molcel.2020.02.021. Epub 2020 Mar 12. PMID: 32169162.boumd

[39] Ralf Metzler and Joseph Klafter. The random walk's guide to anomalous diffusion: a fractional dynamics approach. Physics reports, 339(1):1-77, 2000.

[40] L Bruno, V Levi, M Brunstein, and MA Desposito. Transition to superdiffusive behavior in intracellular actin-based transport mediated by molecular motors. Physical Review E, 80(1):011912, 2009.

[41] Stephanie C Weber, Andrew J Spakowitz, and Julie A Theriot. Bacterial chromosomal loci move subdiffusively through a viscoelastic cytoplasm. Physical review letters, 104(23):238102, 2010.

[42] Bellelli, R. & Boulton, S. J. Spotlight on the Replisome: Aetiology of DNA Replication-Associated Genetic Diseases. *Trends Genet* **37**, 317-336, doi:10.1016/j.tig.2020.09.008 (2021).

[43] Rahman, N. Realizing the promise of cancer predisposition genes. *Nature* **505**, 302-308, doi:10.1038/nature12981 (2014).

[44] Ciccia, A. & Elledge, S. J. The DNA damage response: making it safe to play with knives. Mol Cell 40, 179-204, doi:10.1016/j.molcel.2010.09.019 (2010).

[45] Bartek, J., Lukas, J. & Bartkova, J. DNA damage response as an anti-cancer barrier: damage threshold and the concept of 'conditional haploinsufficiency'. Cell Cycle 6, 2344-2347, doi:10.4161/cc.6.19.4754 (2007).

[46] Tokunaga, M., Imamoto, N. & Sakata-Sogawa, K. Highly inclined thin illumination enables clear single-molecule imaging in cells. *Nat Methods* **5,** 159–161 (2008). https://doi.org/10.1038/nmeth1171

[47] Tinevez JY, Perry N, Schindelin J, Hoopes GM, Reynolds GD, Laplantine E, Bednarek SY, Shorte SL, Eliceiri KW. TrackMate: An open and extensible platform for single-particle tracking. Methods. 2017 Feb 15;115:80-90. doi: 10.1016/j.ymeth.2016.09.016. Epub 2016 Oct 3. PMID: 27713081.

[48] John C. Crocker, David G. Grier, Methods of Digital Video Microscopy for Colloidal Studies, Journal of Colloid and Interface Science, 1996, 298-310, https://doi.org/10.1006/jcis.1996.0217.

[49] Loh W-T, Voo KHB, Bong DBL. Video quality assessment based on a modified mean squared error. 2015 IEEE International Conference on Signal and Image Processing Applications (ICSIPA). Published online October 2015. doi:10.1109/icsipa.2015.7412242

[50] What is Signal to Noise Ratio and How to calculate it. What is Signal to Noise Ratio and How to calculate it? Cadence.com. Published January 29, 2020. Accessed June 2, 2021. https://resources.pcb.cadence.com/blog/2020-what-is-signal-to-noise-ratio-and-how-to-calculate-it

[51] Selecting Fluorescent Dyes. Ucsd.edu. Published 2020. Accessed June 2, 2021. https://nic.ucsd.edu/tips/dyes.html

[52] Ng PC, Henikoff S. SIFT: Predicting amino acid changes that affect protein function. *Nucleic Acids Res*. 2003;31(13):3812-3814. doi:10.1093/nar/gkg509

[53] Schneider TD, Stormo GD, Gold L, Ehrenfeucht A. Information content of binding sites on nucleotide sequences. J Mol Biol. 1986 Apr 5;188(3):415-31. doi: 10.1016/0022-2836(86)90165-8. PMID: 3525846.

[54] Ramensky V, Bork P, Sunyaev S. Human non-synonymous SNPs: server and survey. Nucleic Acids Res. 2002 Sep 1;30(17):3894-900. doi: 10.1093/nar/gkf493. PMID: 12202775; PMCID: PMC137415.

[55] Woringer M, Darzacq X. Protein motion in the nucleus: from anomalous diffusion to weak interactions. Biochem Soc Trans. 2018 August 20;46(4):945-956. Doi: 10.1042/BST20170310. Epub 2018 Jul 31. PMID: 30065106; PMCID: PMC6103463.

[56] Mulvihill DP. Live Cell Imaging in Fission Yeast. *Cold Spring Harbor Protocols.* 2017;2017(10):pdb.top090621. doi 10.1101/pdb.top090621

[57] Shashkova S, Leake MC. Single-Molecule fluorescence microscopy review: shedding new lights on old problems. Biosci Rep. 2017 Jul 21;37(4):BSR20170031. Doi: 10.1042/ BSR20170031. PMID: 28694303; PMCID: PMC5520217.

[58] Bu P, Nagar S, Bhagwat M, et al. The DNA damage response activates respiration and thereby enlarges dNTP pools to promote cell survival in budding yeast. Journal of Biological Chemistry. Published online May 9, 2019:jbc.RA118.007266. doi:10.1074/jbc.RA118.007266

[59] Zhao, X., Muller, E. G., and Rothstein, R. (1998) A suppressor of two essential checkpoint genes identifies a novel protein that negatively affects dNTP pools. Mol. Cell 2, 329–340

[60] Zhao, X., Chabes, A., Domkin, V., Thelander, L., and Rothstein, R. (2001) The ribonucleotide reductase inhibitor Sml1 is a new target of the Mec1/ Rad53 kinase cascade during growth and in response to DNA damage. EMBO J. 20, 3544–3553

[61] Zhao, X., and Rothstein, R. (2002) The Dun1 checkpoint kinase phosphorylates and regulates the ribonucleotide reductase inhibitor Sml1. Proc. Natl. Acad. Sci. U.S.A. 99, 3746–3751

[62] Andreson, B. L., Gupta, A., Georgieva, B. P., and Rothstein, R. (2010) The ribonucleotide reductase inhibitor, Sml1, is sequentially phosphorylated, ubiquitylated and degraded in response to DNA damage. Nucleic Acids Res. 38, 6490–6501

[63] Clerici M, Paciotti V, Baldo V, Romano M, Lucchini G, Longhese MP. Hyperactivation of the yeast DNA damage checkpoint by TEL1 and DDC2 overexpression. EMBO J. 2001 Nov 15;20(22):6485-98. doi: 10.1093/emboj/20.22.6485. PMID: 11707419; PMCID: PMC125310.

[64] DaSilva LF, Pillon S, Genereaux J, Davey MJ, Gloor GB, Karagiannis J, Brandl CJ. The C-terminal residues of Saccharomyces cerevisiae Mec1 are required for its localization, stability, and function. G3 (Bethesda). 2013 Oct 3;3(10):1661-74. doi: 10.1534/g3.113.006841. PMID: 23934994; PMCID: PMC3789791.

[65] Lemaître C, Grabarz A, Tsouroula K, et al. Nuclear position dictates DNA repair pathway choice. *Genes Dev*. 2014;28(22):2450-2463. doi:10.1101/gad.248369.114

[66] Harko T, Mocanu G. Electromagnetic radiation of charged particles in stochastic motion. The European Physical Journal C. 2016;76(3). doi:10.1140/epjc/s10052-016-4009-9

[67] Zheng Q, Ayala AX, Chung I, et al. Rational Design of Fluorogenic and Spontaneously Blinking Labels for Super-Resolution Imaging. *ACS Central Science*. 2019;5(9):1602-1613. doi:10.1021/acscentsci.9b00676

[68] Boothe T, Lennart Hilbert, Heide M, et al. A tunable refractive index matching medium for live imaging cells, tissues and model organisms. eLife. Published July 14, 2017. https://elifesciences.org/articles/27240; eLife 2017;6:e27240; DOI: 10.7554/eLife.27240

APPENDICES

Appendix I: List of yeast Strains

Name	Description	Mating	Genotype
WT BY4743	Diploid wild-type	MATa/α	MAT*a/α* his3*Δ*1/his3*Δ*1 leu2*Δ*0/leu2*Δ*0 LYS2/lys2*Δ*0 met15*Δ*0/MET15 ura3*Δ*0/ura3*Δ0*
YJL11	Pol32-Halo in PCNA-mNG and pdr5Δ0 background, dissected from YSW93	MATα	MAT*α his3Δ1 leu2Δ0 lys2Δ0 MET15 ura3Δ0 pdr5Δ0-Kan PCNA-mNeonGreen-Nat POL32-Halo-HygB*
ZEY206	Rfa1-Halo in Δpdr5 PCNA-mNG, dissected from ZEY196	MATa	MATa his3*Δ*1 leu2*Δ*0 LYS2 met15*Δ*0 ura3*Δ0 RFA1-Halo-HygB POL30-mNeonGreen-Nat Δpdr5::KanMX*
YTK1434	Histone H3 HHT1-HaloTag::URA3. PDR5-delta mutation.	MAT a	MATa his3Δ1 leu2Δ0 met15Δ0 ura3Δ0 pdr5Δ::LoxP-KAN-LoxP HHT1-HaloTag::URA3
YSR18	DDC2-Halo. PCR from pSJW01 using SR17/SR18 and transformed into BY4743	MATa/α	MAT*a/α* his3*Δ*1/his3*Δ*1 leu2*Δ*0/leu2*Δ*0 LYS2/lys2*Δ*0 met15*Δ*0/MET15 ura3*Δ*0/ura3*Δ0 DDC2/DDC2-Halo-HygB*
YSR19	DUN1-Halo. PCR from pSJW01 using SR21/SR22 and transformed into BY4743	MATa/α	MAT*a/α* his3*Δ*1/his3*Δ*1 leu2*Δ*0/leu2*Δ*0 LYS2/lys2*Δ*0 met15*Δ*0/MET15 ura3*Δ*0/ura3*Δ0 DUN1/DUN1-Halo-HygB*
YSR30	TEL1-Halo. PCR from pSJW01 using SR13/SR14 and transformed into BY4743	MATa/α	MAT*a/α* his3*Δ*1/his3*Δ*1 leu2*Δ*0/leu2*Δ*0 LYS2/lys2*Δ*0 met15*Δ*0/MET15 ura3*Δ*0/ura3*Δ0 TEL1/TEL1-Halo-HygB*
YSR31	DDC2-Halo. PCR from pSJW01 using SR17/SR18 and	MATa/α	MAT*a/α* his3*Δ*1/his3*Δ*1 leu2*Δ*0/leu2*Δ*0 LYS2/lys2*Δ*0

	transformed into BY4743		met15*Δ*0/MET15 ura3*Δ*0/ura3*Δ0 DDC2/DDC2-Halo-HygB*
YSR32	DUN1-Halo. PCR from pSJW01 using SR21/SR22 and transformed into BY4743	MATa/α	MAT*a/α* his3*Δ*1/his3*Δ*1 leu2*Δ*0/leu2*Δ*0 LYS2/lys2*Δ*0 met15*Δ*0/MET15 ura3*Δ*0/ura3*Δ0 DUN1/DUN1-Halo-HygB*
YSR36	Rad53-Halo. PCR from pSJW01 using SR05/SR06 and transformed into BY4743	MATa/α	MAT*a/α* his3*Δ*1/his3*Δ*1 leu2*Δ*0/leu2*Δ*0 LYS2/lys2*Δ*0 met15*Δ*0/MET15 ura3*Δ*0/ura3*Δ0 RAD53/RAD53-Halo-HygB*
YSR37	Rad53-Halo. PCR from pSJW01 using SR05/SR06 and transformed into BY4743	MATa/α	MAT*a/α* his3*Δ*1/his3*Δ*1 leu2*Δ*0/leu2*Δ*0 LYS2/lys2*Δ*0 met15*Δ*0/MET15 ura3*Δ*0/ura3*Δ0 RAD53/RAD53-Halo-HygB*

Table A1: List of all the strains used for all the above-mentioned experiments with their genotype and description

Appendix II: List of Plasmids

Plasmid	**Description**
pSJW01	HaloTag Gene with HygB selectable marker
pH6HTC	Histone HaloTag Plasmid
pKD4	Kanamycin resistant gene Plasmid
pUC18	Vector Plasmid
pML104	Cas9-sgRNA expression vector with the *URA3* selectable marker
pML107	Cas9-sgRNA expression vector with the *LEU2* selectable marker

Table A2: List of all the plasmids for the strain construction and their description

Appendix III: Oligonucleotides Sequences

- **For plasmid cloning**

Name	Description	Sequence
Halo C-ter-F	Cloning Halo tag for C-ter fusions through l-red	AGGAGCTCGGCTGGCTCCGCTGCTGGTTCTGGCGCAGTCGGATCCGAAATCGGTACTGG
Halo C-ter-R	Cloning Halo tag for C-ter fusions through l-red	TTTaccggtTTAACCGGAAATCTCCAGAGTAG
Halo seq3'	Screening integrated halo gene-fusions	AAGCCTGCCTAACTGCAAGG
Halo seq5'	Screening integrated halo gene-fusions	CATCGCGCGGACCAACATC
Halo_NF	For cloning FPs for N-terminal fusions for Histone HaloTag Plasmid	TTTaccggtATGGGATCCGAAATCGGTACTGG
Halo_NR	For cloning FPs for N-terminal fusions for Histone HaloTag Plasmid	AGGAGCTCGCGCTGCCAGAACCAGCGGCGGAGCCTGCCGAACCGGAAATCTCCAGAGTAG
Kan_nfus_R	For cloning FPs for N-terminal fusions	TTAGGATCCTGTAGGCTGGAGCTGCTTCG
Kan_nfus_F	For cloning FPs for N-terminal fusions	TTACCCGGGCATATGAATATCCTCCTTAG

Table A3: List of all the oligonucleotides required for Plasmid cloning

- **For strain construction**

Name	Description	Sequence
SR05	Forward primer to tag RAD53 with FP	GGACCAAACCTCAAAAGGCCCCGAGAATT TGCAATTTTCGggtgacggtgctggtttaat
SR06	Reverse primer to tag RAD53 with FP	TTAAAAAGGGGCAGCATTTTCTATGGGTAT TTGTCCTTGGcagtatagcgaccagcattc
SR07	Forward primer to ampllify C-ter insertion at RAD53 locus.	CGATACAAATAATAACGGC
SR08	Rev primer to ampllify C-ter insertion at RAD53 locus.	AACTAAAACTGAAAATCAAAAC
SR09	For primer to tag MEC1 with FP	CAATCTAAGCAAGATGTATATTGGTTGGCT TCCATTTTGGggtgacggtgctggtttaat
SR10	Rev primer to tag MEC1 with FP	AAGAGGAAGTTCGTCTGTTGCCGAAAATG GTGGAAAGTCGcagtatagcgaccagcattc
SR11	For primer to ampllify C-ter insertion at MEC1 locus.	GCGTTGATGAATGTGATCG
SR12	Rev primer to ampllify C-ter insertion at MEC1 locus.	GCTTGATTAGGTTGTTTCTC
SR13	For primer to tag TEL1 with FP	AAATTTGAGTGTTATATATATGGGATGGTC ACCTTTTTATggtgacggtgctggtttaat

SR14	Rev primer to tag TEL1 with FP	TATAAACAAAAAAAAGAAGTATAAAGCATC TGCATAGCAAcagtatagcgaccagcattc
SR15	For primer to ampllify C-ter insertion at TEL1 locus.	AAGTAACAACGACAGGAACG
SR16	Rev primer to ampllify C-ter insertion at TEL1 locus.	CCAAATCTGCGTAGTGAGTC
SR17	For primer to tag DDC2 with FP	ACTAGAGGAGGCCGATTCATTATATATCTC AATGGGACTGggtgacggtgctggtttaat
SR18	Rev primer to tag DDC2 with FP	TTCTATAAAGCGTTGACATTTTCCCCTTTTG ATTGTTGCCcagtatagcgaccagcattc
SR19	For primer to ampllify C-ter insertion at DDC2 locus.	GCCTTTGAGGATTTACCAGA
SR20	Rev primer to ampllify C-ter insertion at DDC2 locus.	GAAGTTGTTCTGAATCCAGC
SR21	For primer to tag DUN1 with FP	CAATAAAATACCCAAAACATACTCAGAATT ATCTTGCCTCggtgacggtgctggtttaat
SR22	Rev primer to tag DUN1 with FP	CCAGATTCAAACAATGTTTTTGAAATAATG CTTCTCATGTcagtatagcgaccagcattc
SR23	For primer to ampllify C-ter insertion at DUN1 locus.	TCTTACAAGCTAAGTATGCG

SR24	Rev primer to ampllify C-ter insertion at DUN1 locus.	CGTTGAGGAAAGGTGAAGG
SR29	N Terminal gRNA for mec1	GGCAATAAAAGACCTGAACTCGG
SR30	N Terminal Oligo1 for Mec1	GATCGGCAATAAAAGACCTGAACTGTTTTAGAGCTAG
SR31	N terminal Oligo2 for Mec1	CTAGCTCTAAAACAGTTCAGGTCTTTTATTGCC
SR32	N terminal gRNA for Tel1	TATATAACACTCAAATTTGATGG
SR33	N terminal Oligo1 for Tel1	GATCTATATAACACTCAAATTTGAGTTTTAGAGCTAG
SR34	N terminal Oligo2 for Tel1	CTAGCTCTAAAACTCAAATTTGAGTGTTATATA

Table A4: List of all the nucleotides required for strain construction

Appendix IV: HaloTag Fluorescent dyes

1. PA-JF549
2. PA-JF646
3. JF552
4. JF646

Appendix V: Analysis of Nuclear Movement in Budding Yeast

Budding yeast VS Fission yeast

G1 phase

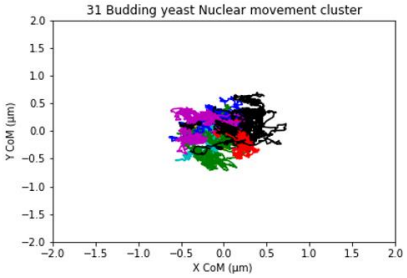

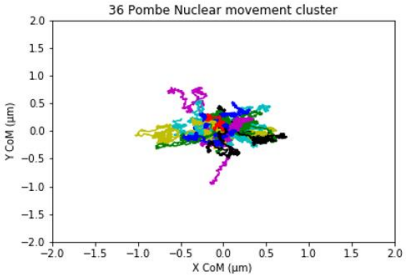

S/G2 phase

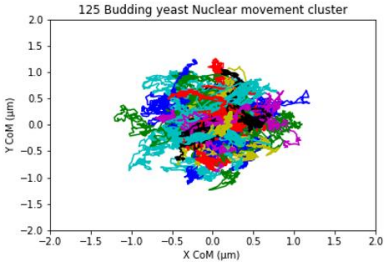

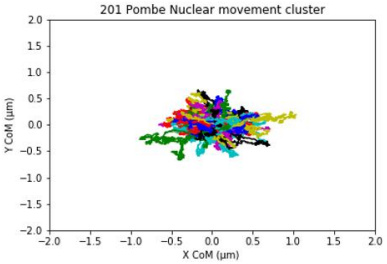

App V (a): Cluster graph

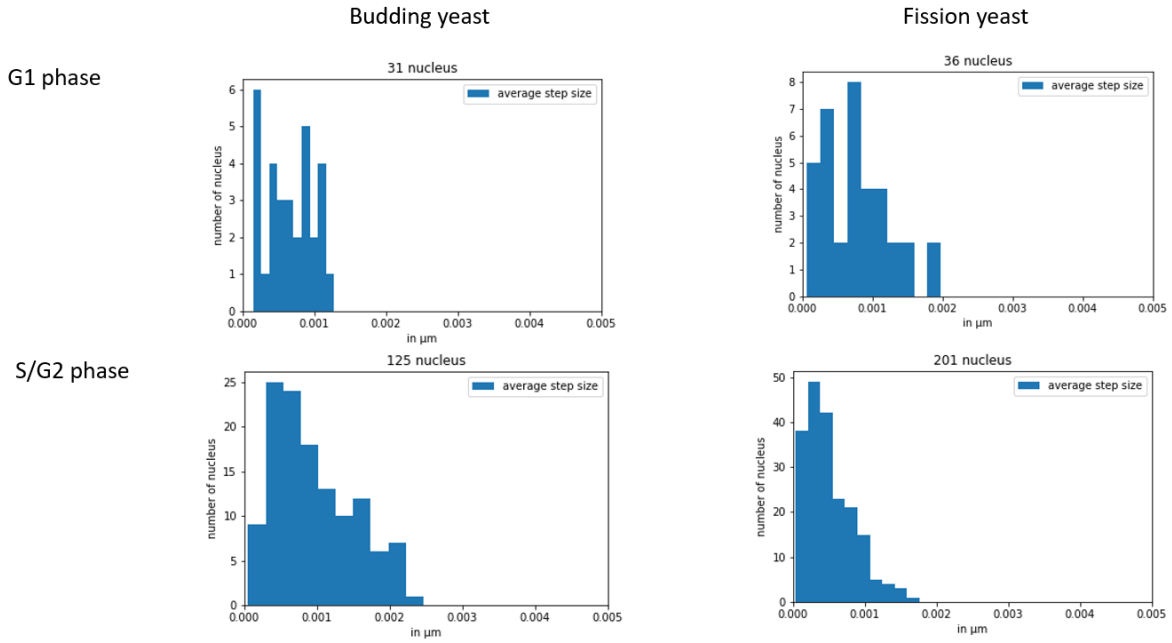

App V(b): Average step size

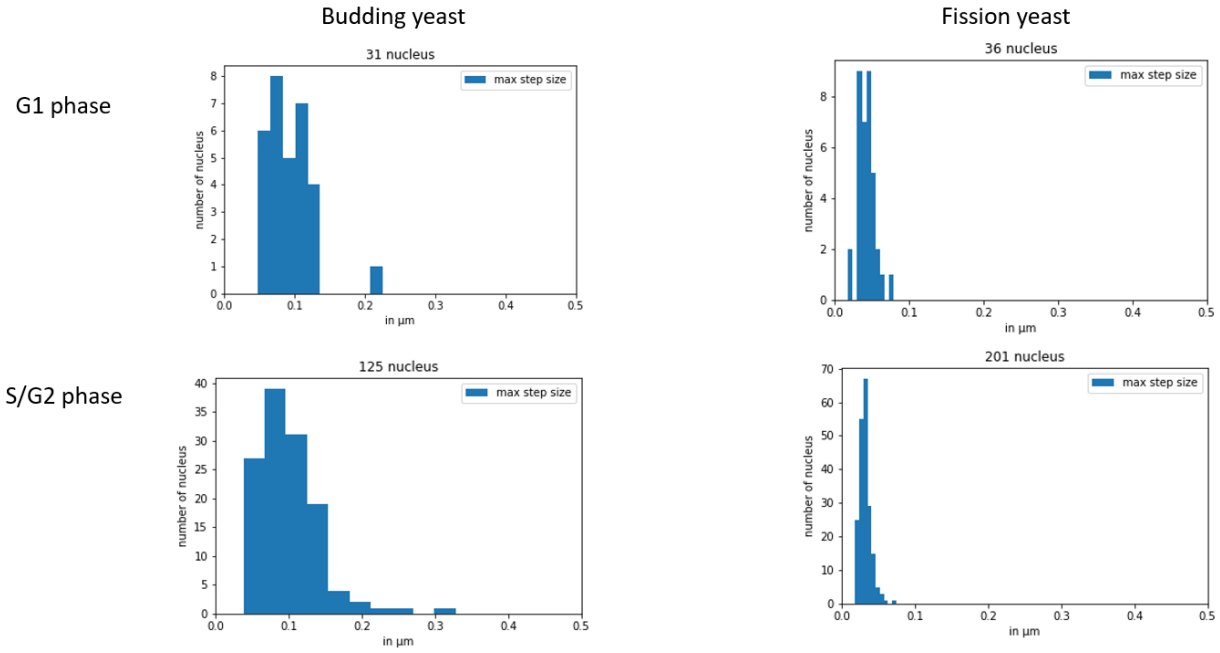

App V(c): Maximum step size

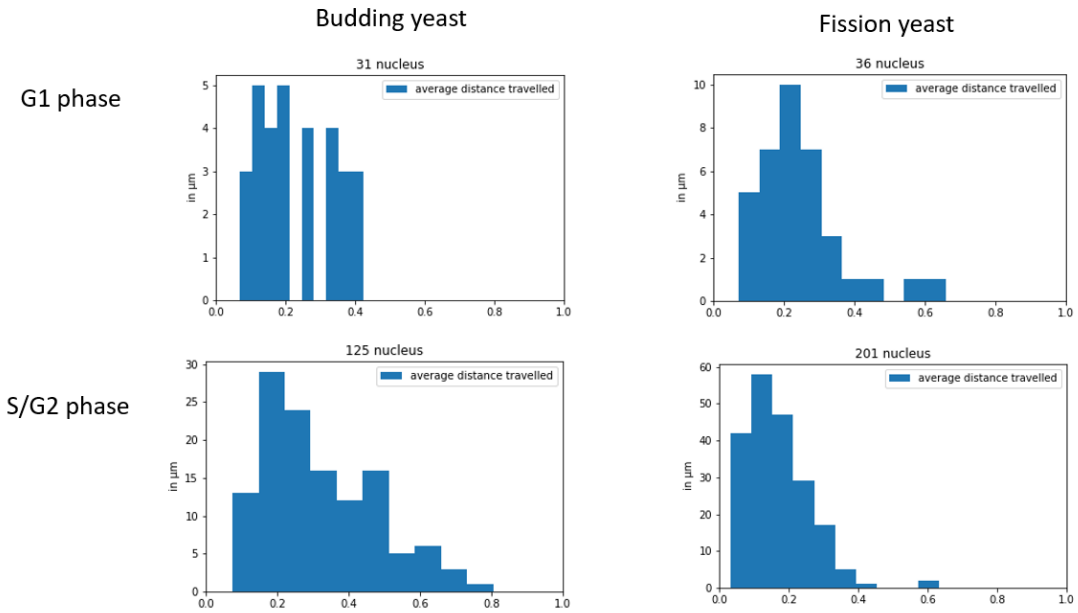

App V(d): Maximum distance travelled

Untreated and Treated Budding Yeast

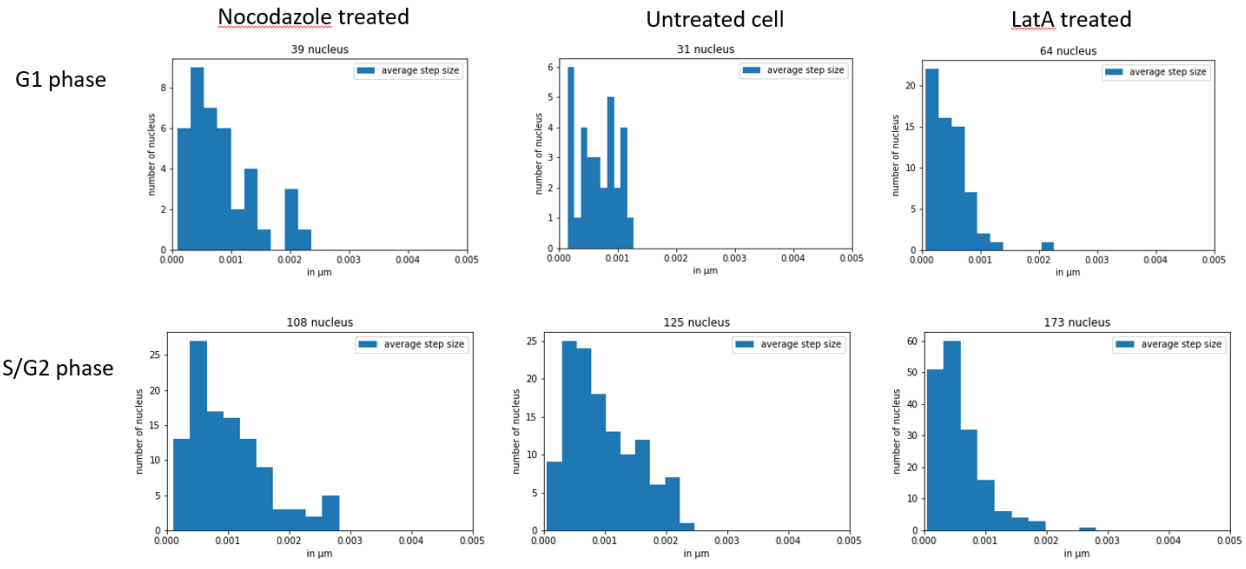

App V(e): Average step size

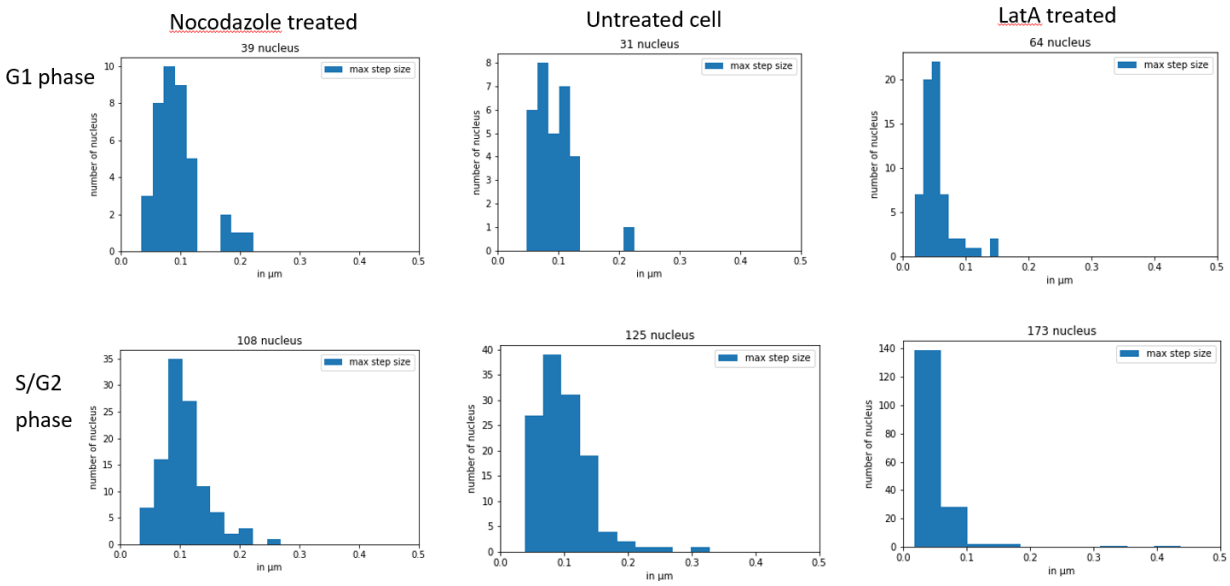

App V(f): Maximum step size

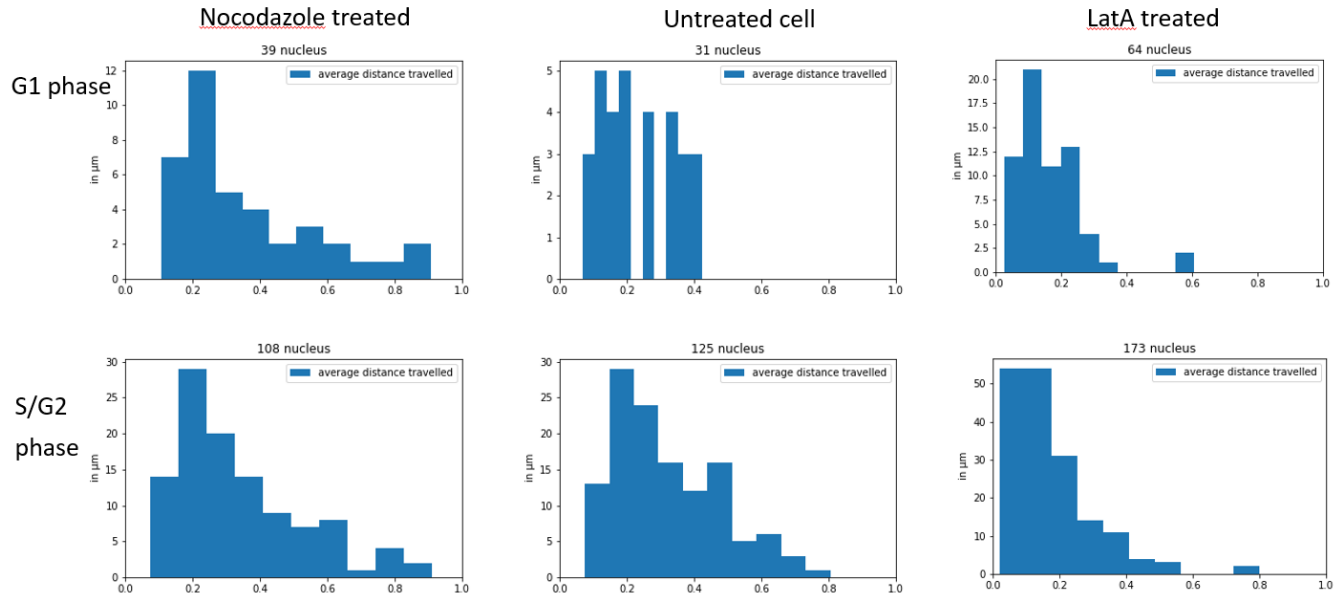

App V(g): Maximum distance travelled

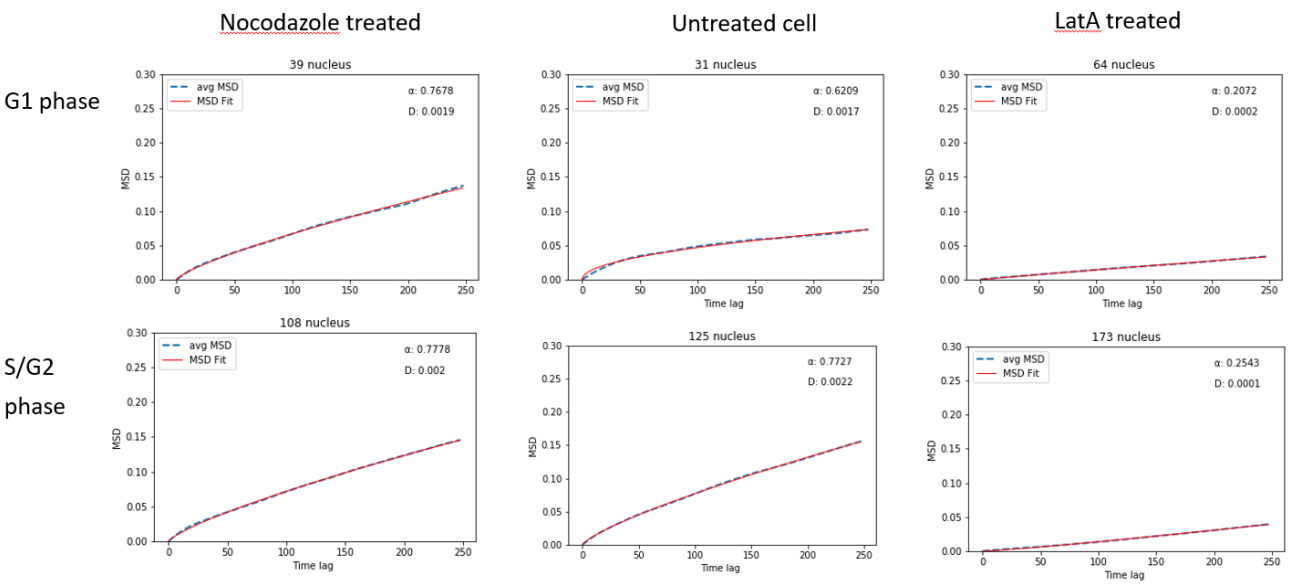
Nocodazole treated
Untreated cell
LatA treated
G1 phase
S/G2 phase
39 nucleus
α: 0.7678
D: 0.0019
31 nucleus
α: 0.6209
D: 0.0017
64 nucleus
α: 0.2072
D: 0.0002
108 nucleus
α: 0.7778
D: 0.002
125 nucleus
α: 0.7727
D: 0.0022
173 nucleus
α: 0.2543
D: 0.0001
avg MSD
MSD Fit
MSD
Time lag

App V(h): MSD

Appendix VI: Analysis of experiments with different fluorophores and different growth conditions

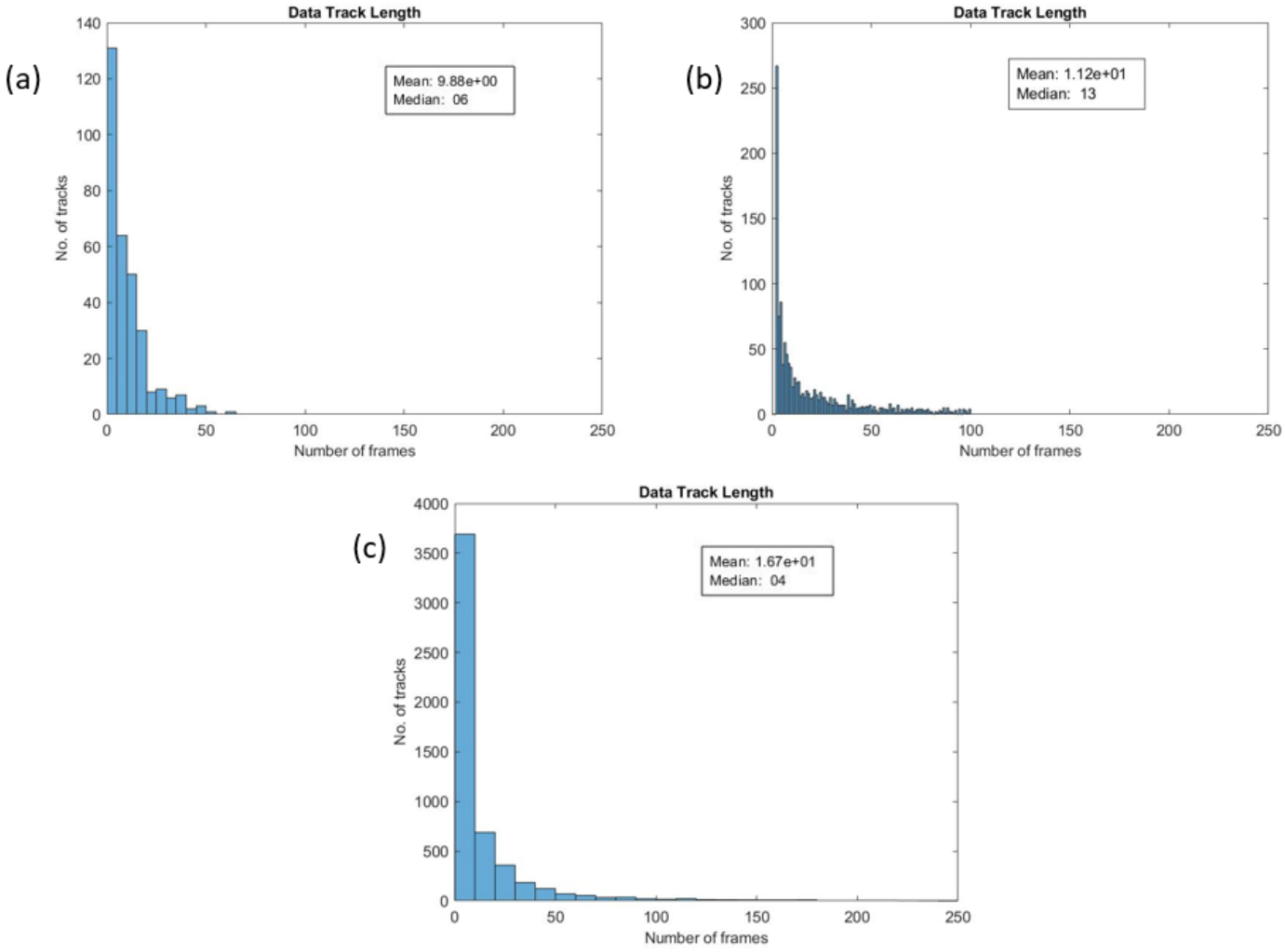

App VI (1): JF552 Track Length Analysis (a) ConA growth condition (b) Optiprep with Agarose Growth Condition (c) Optiprep with SC Growth Condition

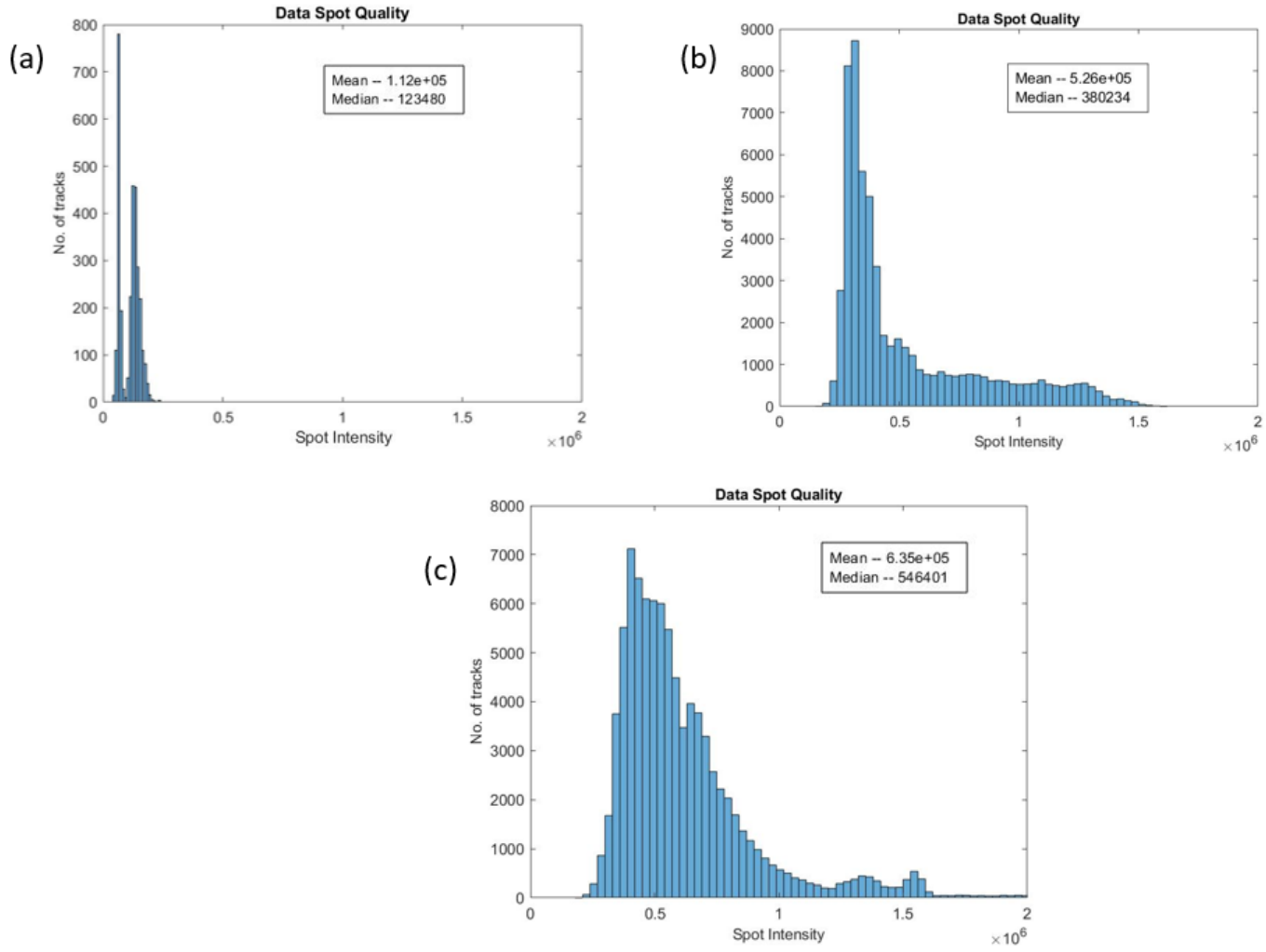

App VI (2): JF552 Spot qulaity Analysis (a) ConA growth condition (b) Optiprep with Agarose Growth Condition (c) Optiprep with SC Growth Condition

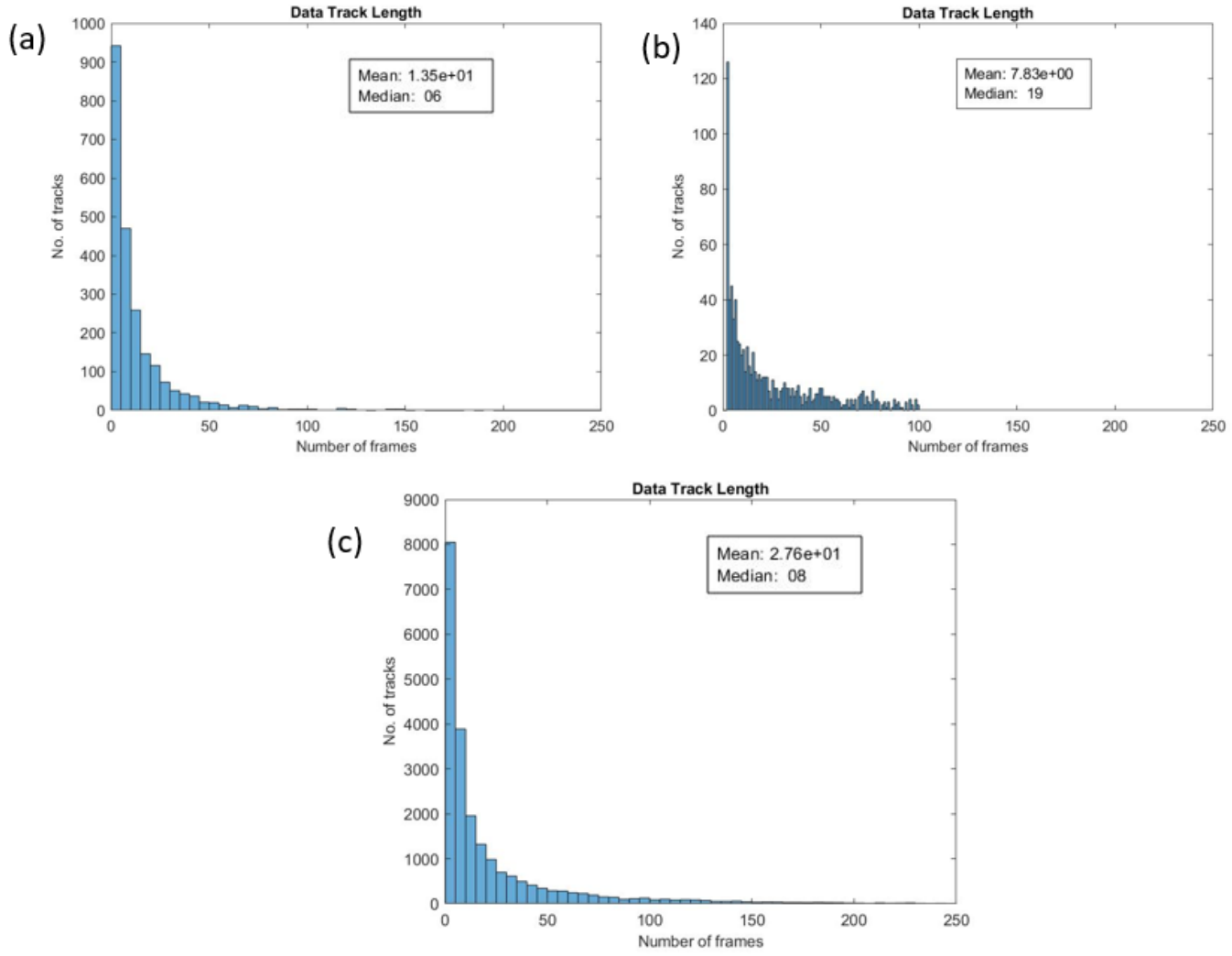

App VI (3): JF646 Track Length Analysis (a) ConA growth condition (b) Optiprep with Agarose Growth Condition (c) Optiprep with SC Growth Condition

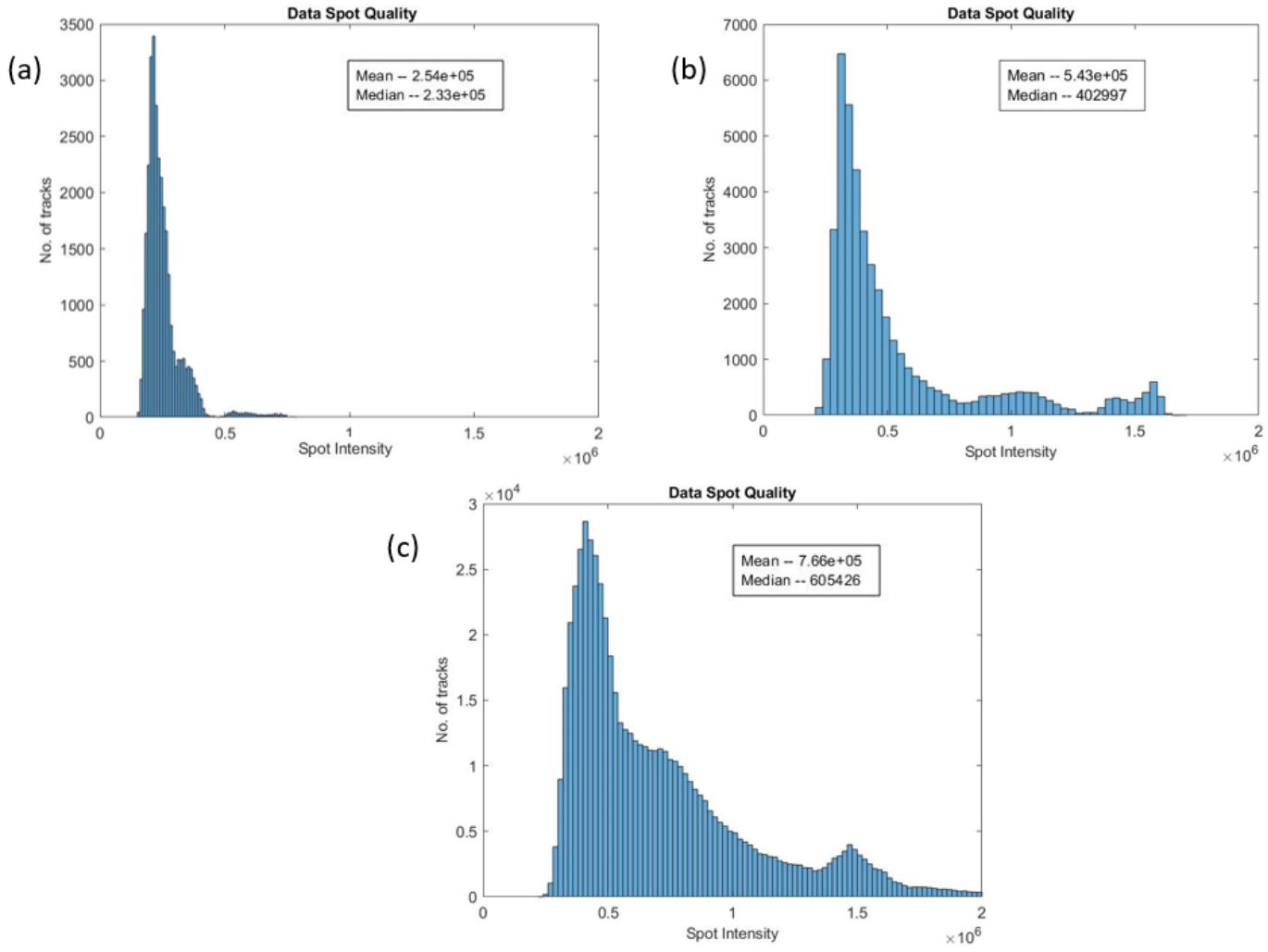

App VI (4): JF646 Spot Qulaity Analysis (a) ConA growth condition (b) Optiprep with Agarose Growth Condition (c) Optiprep with SC Growth Condition

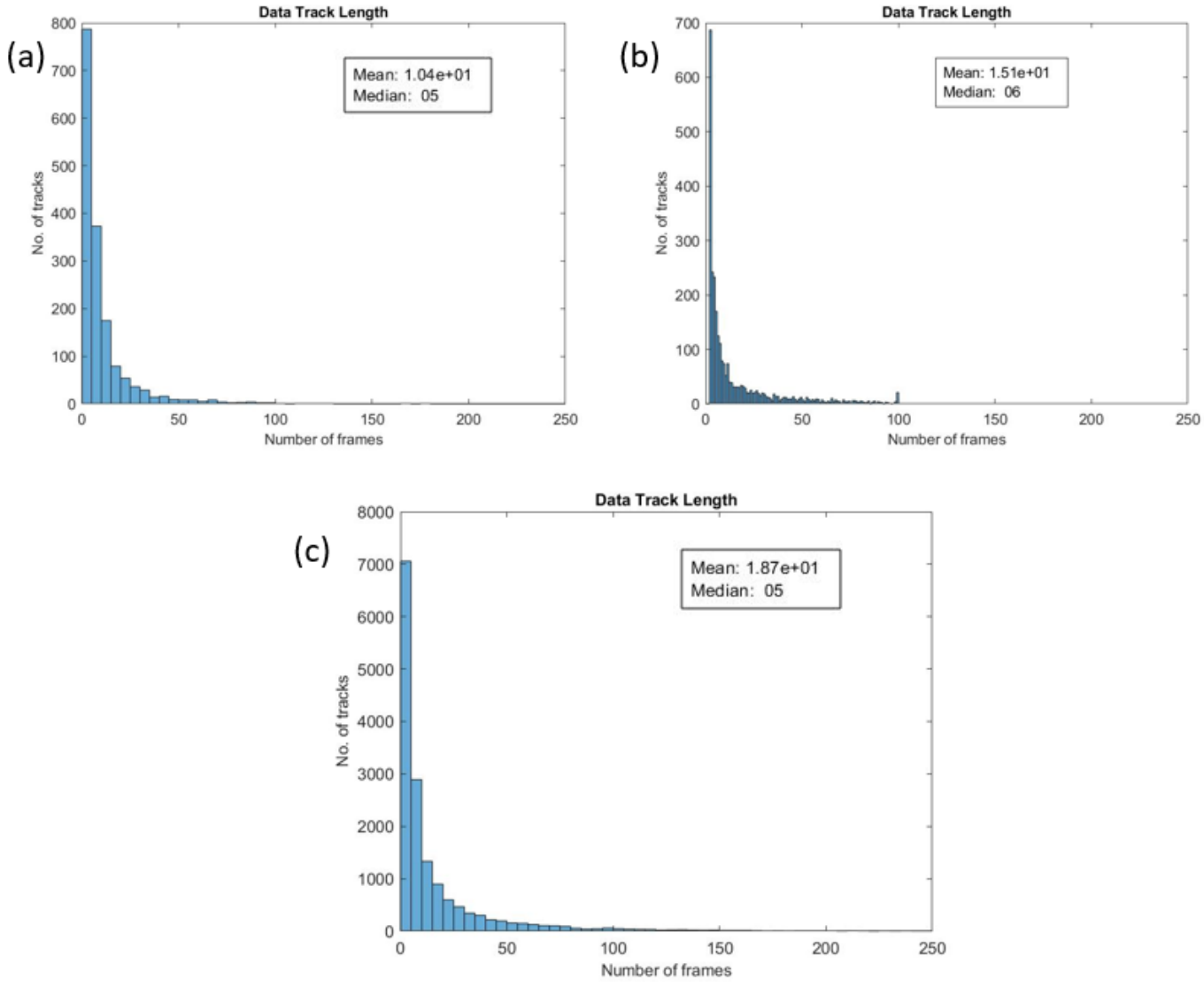

App VI (5): PA-JF549 Track Length Analysis (a) ConA growth condition (b) Optiprep with Agarose Growth Condition (c) Optiprep with SC Growth Condition

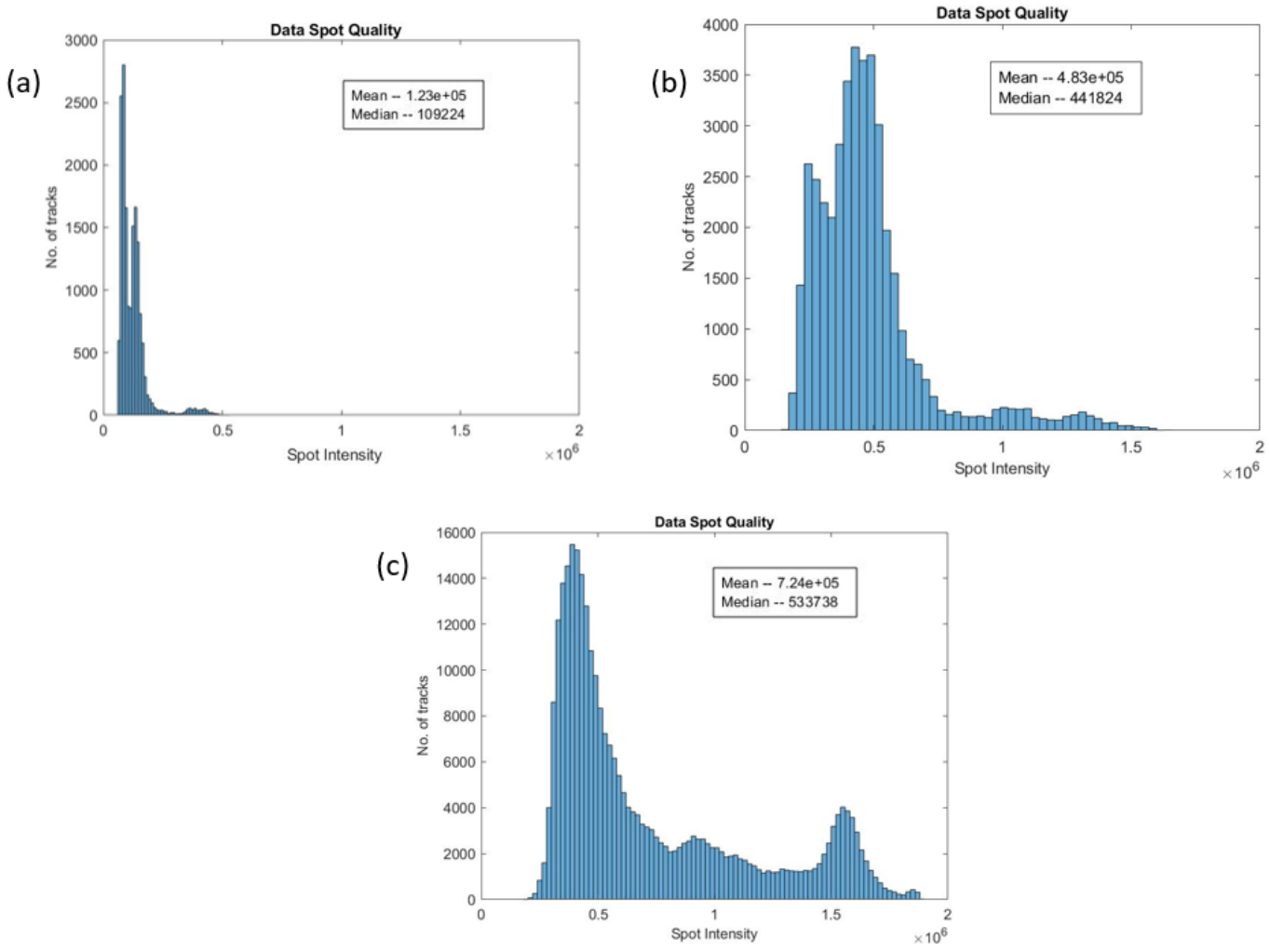

App VI (6): PA-JF549 Spot Quality Analysis (a) ConA growth condition (b) Optiprep with Agarose Growth Condition (c) Optiprep with SC Growth Condition

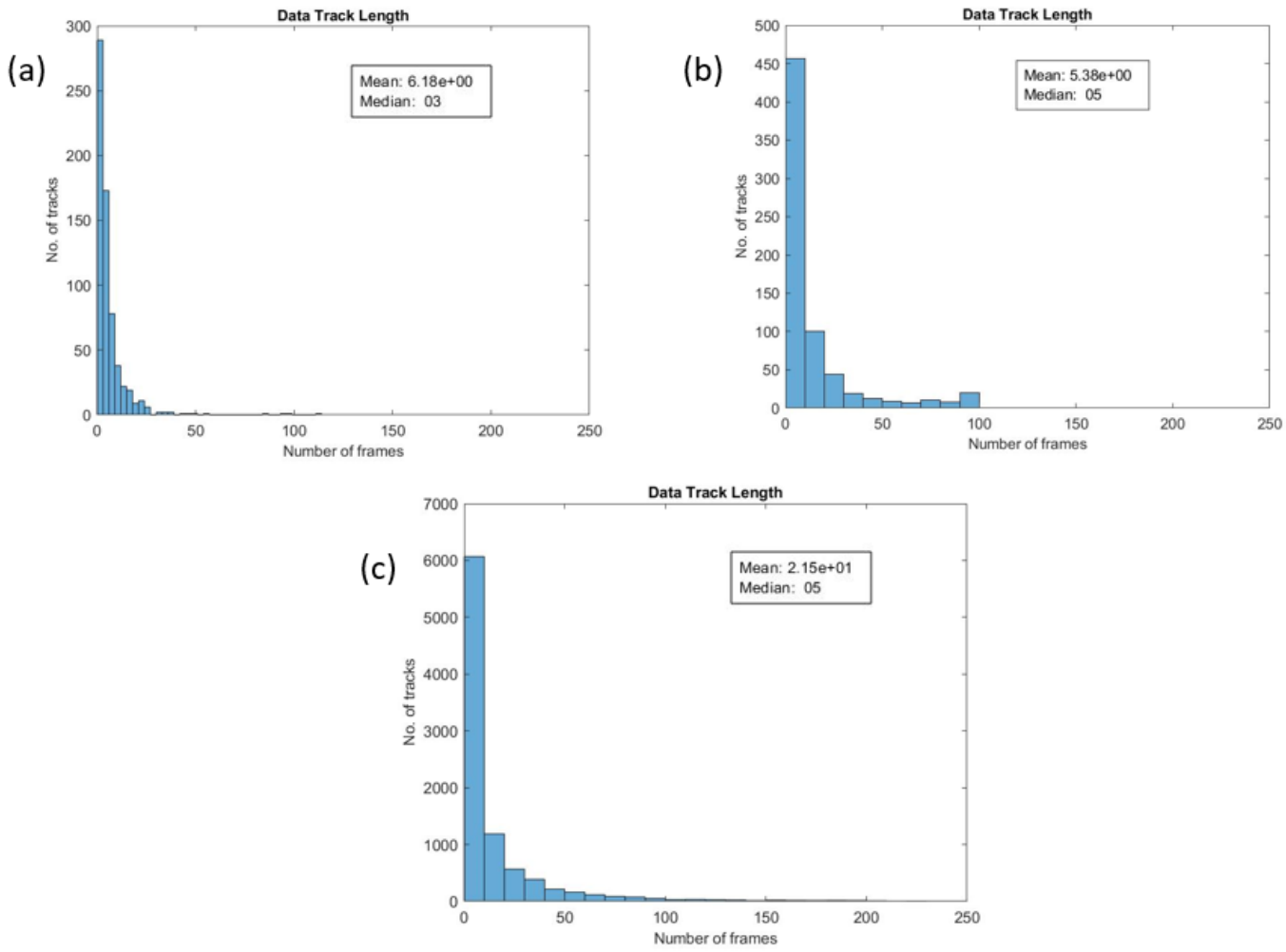

App VI (7): PA-JF646 Track Length Analysis (a) ConA growth condition (b) Optiprep with Agarose Growth Condition (c) Optiprep with SC Growth Condition

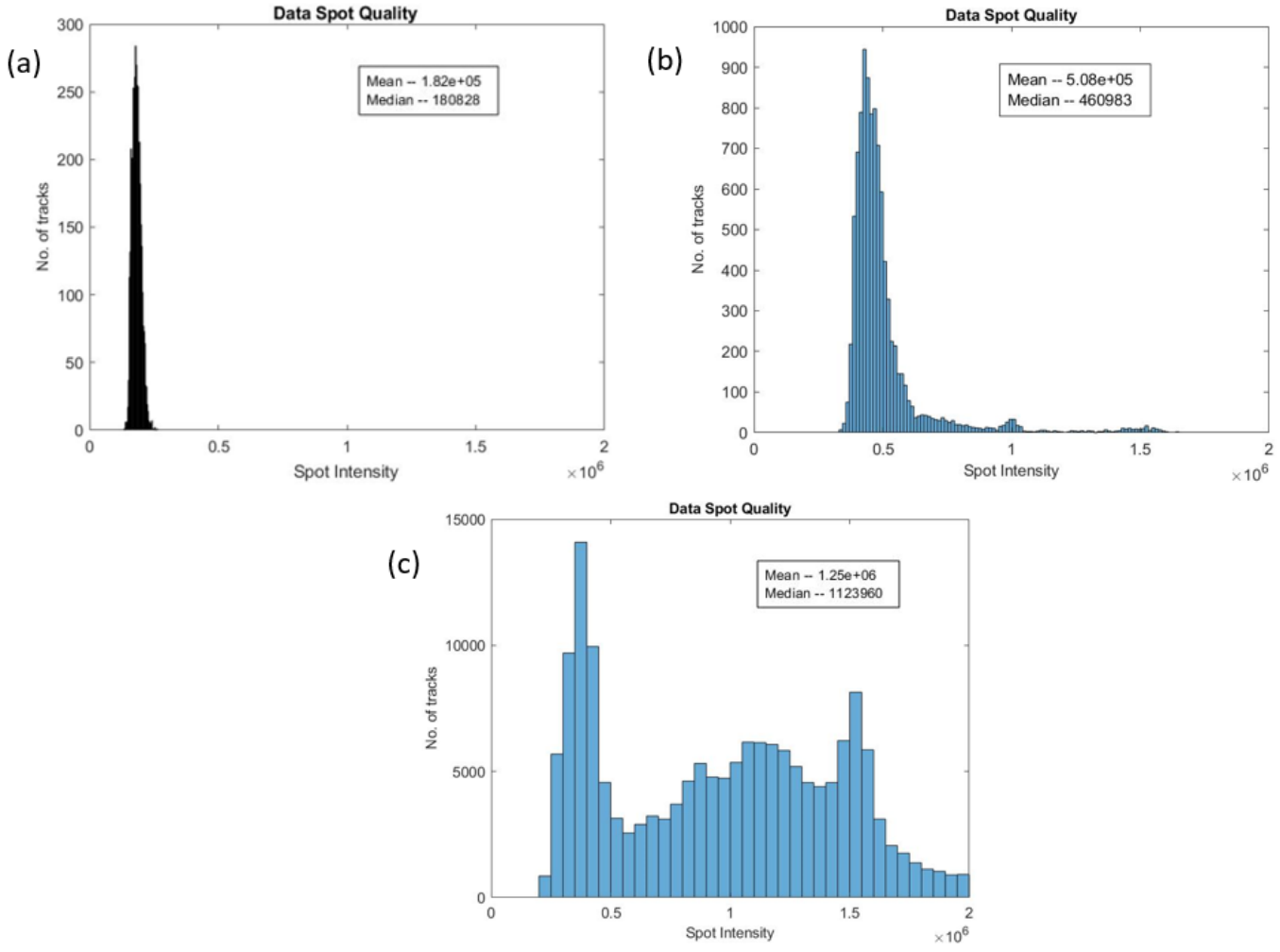

App VI (8): PA-JF646 Spot Quality Analysis (a) ConA growth condition (b) Optiprep with Agarose Growth Condition (c) Optiprep with SC Growth Condition

Appendix VII: DDR variants Bioinformatic Analysis

SIFT Scoring: Mec1

Variant ID	sift_class	SIFT
s02-507058	deleterious	0.02
s02-507213	tolerated	0.26
s02-507268	tolerated	0.66
s02-507661	tolerated	0.43
s02-507790	tolerated	0.6
s02-507802	tolerated	0.78
s02-508249	deleterious	0.03
s02-510134	tolerated	0.54
s02-510231	tolerated	1
s02-510351	tolerated	0.96
s02-510427	tolerated	1
s02-510436	tolerated	0.56
s02-510694	tolerated	0.5
s02-512080	deletorious	0.01

SIFT Scoring: RAD53

Variant ID	sift_class	SIFT
s16-261905	tolerated - low confidence	0.84

s16-262451	tolerated	0.58
s16-262501	tolerated	0.67
s16-263633	tolerated	0.63
s16-263634	tolerated	0.2
s16-263634	tolerated	0.2
s16-263647	tolerated	0.14
s16-263732	tolerated	0.76

SIFT Scoring: TEL1

Variant ID	**sift_class**	**SIFT**
s02-53145	tolerated - low confidence	1
s02-53150	tolerated - low confidence	0.82
s02-53579	tolerated - low confidence	0.31
s02-53582	tolerated - low confidence	0.5
s02-53799	deleterious - low confidence	0
s02-53850	deleterious - low confidence	0.02
s02-54054	tolerated - low confidence	0.82
s02-54153	tolerated - low confidence	0.88
s02-54264	tolerated - low confidence	1
s02-54335	tolerated - low confidence	0.33

s02-59043	tolerated - low confidence	0.5
s02-59188	tolerated - low confidence	1
s02-59196	tolerated - low confidence	0.2
s02-59274	deleterious - low confidence	0

SIFT Scoring: DDC2

Variant ID	**sift_class**	**SIFT**
s04-1447829	tolerated - low confidence	0.81
s04-1447869	tolerated - low confidence	0.46
s04-1447935	tolerated	0.09
s04-1447951	tolerated	0.75
s04-1447954	tolerated	0.81
s04-1448092	tolerated	0.27
s04-1448333	tolerated - low confidence	0.34
s04-1448512	tolerated	0.33
s04-1448578	tolerated	0.19
s04-1448737	tolerated	1
s04-1448837	tolerated	0.74
s04-1449115	tolerated	1
s04-1449164	tolerated	0.34
s04-1449398	tolerated	0.59
s04-1449421	tolerated - low confidence	0.68
s04-1449917	tolerated	0.64
s04-1450033	tolerated	0.59